THE TRANSFER HAMILTONIAN: A TOOL FOR LARGE SCALE, ACCURATE, MOLECULAR DYNAMICS SIMULATIONS USING QUANTUM MECHANICAL POTENTIALS

By

DECARLOS E. TAYLOR

A DISSERTATION PRESENTED TO THE GRADUATE SCHOOL
OF THE UNIVERSITY OF FLORIDA IN PARTIAL FULFILLMENT
OF THE REQUIREMENTS FOR THE DEGREE OF
DOCTOR OF PHILOSOPHY

UNIVERSITY OF FLORIDA

2004

Copyright 2004

by

DECARLOS E. TAYLOR

ACKNOWLEDGMENTS

I would like to thank Dr. Rodney Bartlett for his guidance and support of my scientific endeavors during my time at the University of Florida. Also, special thanks go to the late Dr. Michael Zerner with whom I worked initially before joining the Bartlett research group.

Very big thanks go to Dr. Keith Runge for his advisement and encouragement on matters of scientific and non-academic interest and for his patience. Also, I thank Drs. Marshall Cory and Ajith Perera for answering (always in a timely fashion) my many questions concerning fortran code or quantum theory in general.

I am grateful to Dr. Yngve Ohrn and Mrs. Judy Parker for their kind words of encouragement and droll senses of humor.

Finally, I would like to acknowledge Ms. Valerie Buie for her unwavering support over the final two years of my graduate studies. Also, I thank Dr. Monde Qhobosheane with whom I shared an apartment for my first five years in Florida.

TABLE OF CONTENTS

Page

ACKNOWLEDGMENTS iii

ABSTRACT vii

OVERVIEW OF DISSERTATION 1

MOLECULAR DYNAMICS 2

Introduction 2
Predictive Simulation 2
Molecular Dynamics Potentials 5
Classical Potentials 5
Two body potentials 6
Three body potentials 8
Quantum Potentials 11
Density functional potentials 13
Semiempirical potentials – Tight binding and NDDO models 13
Conclusion 17

TRANSFER HAMILTONIAN 20

Introduction 20
Theoretical Formulation 20
Coupled Cluster Theory Formulation 22
Density Functional Theory Formulation 25
Functional Form 27
One Center – One Electron Integrals 28
Two Center – One Electron Integrals 29
One Center – Two Electron Repulsion Integrals 30
Two-Center Two Electron Repulsion Integrals 30
Nuclear Repulsion Energy 32
Computational Procedure 32
Parameterization 33
Conclusion 34

EXAMPLE TRANSFER HAMILTONIANS 35

Introduction 35
Parameterization Procedure 35
Genetic Algorithms 35
Newton-Raphson Algorithms 36
Performance Of Algorithms 37
Procedure 39
Transfer Hamiltonian Examples 39
Ethane 39
Disilane 40
Conclusion 42

FRACTURE SIMULATIONS 43

Introduction 43
Fracture 43
Transfer Hamiltonian – Silica 44
Reference Cluster 45
Reference Data For Pyrosilicic Acid 46
Parameterization 47
Validation Of Potential 47
Application 56
Fracture Of Nanorod 56
Hybrid Dynamics Of Nanorod 59
Conclusion 62

HYDROLYTIC WEAKENING 66

Introduction 66
Hydrolytic Weakening 66
Transfer Hamiltonian 68
Parameterization 68
Validation 69
Simulations Of Hydrolytic Weakening 70
Hydrolytic Weakening In Silica Ring 71
Hydrolytic Weakening in Nanorod 73
Conclusion 73

APPENDIX CONVERGED PARAMETER VALUES 79

LIST OF REFERENCES 83

BIOGRAPHICAL SKETCH 88

Abstract of Dissertation Presented to the Graduate School
of the University of Florida in Partial Fulfillment of the
Requirements for the Degree of Doctor of Philosophy

THE TRANSFER HAMILTONIAN: A TOOL FOR LARGE SCALE, ACCURATE, MOLECULAR DYNAMICS SIMULATIONS USING QUANTUM MECHANICAL POTENTIALS

By

DeCarlos E. Taylor

May 2004

Chair: Rodney J. Bartlett
Major Department: Chemistry

The accuracy of a molecular dynamics simulation is contingent upon the quality of the potentials used to compute the intermolecular forces on the constituent atoms. The most accurate potentials are those which result from first principles quantum mechanics computations such as coupled cluster theory; however, for large scale molecular dynamics which may be on the order of 1000's of atoms, this is computationally not feasible as most *ab initio* potentials are limited to 10's or 100's of atoms. In order to avoid this computational bottleneck, the concept of a transfer Hamiltonian is introduced. The transfer Hamiltonian is a low rank, quantum mechanical operator whose matrix elements are computed from parametric functional forms. The parameters which constitute the transfer Hamiltonian are fit to *ab initio* coupled cluster theory results (ionization potentials, geometry, dissociation energies, etc.) for several small model systems which mimic the local structure of the target simulation system. The transfer

Hamiltonian is applicable to systems far beyond the reach of *ab initio* coupled cluster theory, yet it retains the accuracy of the first principles computation. Further, since the transfer Hamiltonian can be rapidly evaluated, it is useful for on-the-fly molecular dynamics simulations and gives results which are more accurate than those obtainable using a classical potential.

CHAPTER 1
OVERVIEW OF DISSERTATION

The focus of this dissertation is the accurate description of molecules and materials using molecular dynamics simulations. Chapter 2 introduces molecular dynamics, defines the term "predictive simulation," and details the reliance of the simulation results on the quality of the potential used. Also, a critique of some existing potentials found in the literature of both classical and quantum forms is given and the necessity for improved potentials delineated.

Chapter 3 introduces the transfer Hamiltonian and discusses its formal foundation in terms of coupled cluster and density functional theories. Following the more formal arguments, the functional form of the operator is outlined and procedures for computation of the matrix elements presented. Representative examples of transfer Hamiltonians for various systems are given in Chapter 4, and a presentation of the parameterization strategy is outlined.

The fifth and sixth chapters contain parameterizations of transfer Hamiltonians applicable to silica and silica in the presence of water respectively. Several tests used to validate the potentials are discussed, and in Chapter 5 a prototypical silicon oxide nanorod is fractured via molecular dynamics using the new quantum and standard classical potentials. Chapter 6 presents simulations of the nanorod in the presence of water and demonstrates the experimentally observable phenomenon known as hydrolytic weakening whereby water causes a dramatic decrease in the strength of silica.

CHAPTER 2
MOLECULAR DYNAMICS

Introduction

This chapter introduces molecular dynamics simulation and defines the term "predictive simulation." Also, an overview of some of the classical and quantum potentials available in the literature, with a focus on those applicable to silica and silicon, is presented. The shortcomings of the available potentials will be discussed and the need for more chemically accurate potentials will be demonstrated.

Predictive Simulation

Molecular dynamics simulations have contributed immensely to the understanding of the chemo-mechanical behavior of large molecules and materials [1]. Given a set of initial conditions (positions and momenta), and the force of interaction among the constituent particles, molecular dynamics computes the phase space trajectories of the particles which constitute the material of interest [2-4]. Given these trajectories, the chemo-mechanical properties of materials and their response to external perturbations can be studied at the atomistic level. The ability to conduct studies with such coarse grained refinement allows researchers to elucidate the underlying reaction mechanisms which determine macroscopic properties.

In classical molecular dynamics, atomic positions are obtained by integrating Newton's equation of motion

$$F_k(t) = m_k \ddot{r}_k(t) = -\frac{\partial V(r)}{\partial r_k} \qquad (2.1)$$

where $F_k(t)$ is the force acting on the kth particle due to the other N-1 nuclei at time t. The particle positions and mass are denoted by r and m respectively and the dots indicate time derivatives. The potential, V(r), determines the interaction among the particles.

These equations are typically solved using finite difference algorithms as analytical solutions are not possible for all but the most simple systems and potential forms [5]. The most efficient and commonly used finite difference algorithms used in molecular dynamics are the Verlet [6] and the Predictor-Corrector algorithms [7]. The quality of any simulation based on either of these algorithms is intrinsically based upon the fidelity of the potential used in the algorithm. As an illustration of this dependence, consider the Verlet algorithm.

The Verlet algorithm is based on a Taylor expansion of the position vector about time t

$$r(t + \Delta t) = r(t) + \dot{r}(\Delta t) + \frac{1}{2}\ddot{r}(\Delta t^2) + \frac{1}{3!}\dddot{r}(\Delta t^3) + \ldots \qquad (2.2)$$

Writing equation 2.2 for $(t - \Delta t)$ yields

$$r(t - \Delta t) = r(t) - \dot{r}(\Delta t) + \frac{1}{2}\ddot{r}(\Delta t^2) - \frac{1}{3!}\dddot{r}(\Delta t^3) + \ldots \qquad (2.2)$$

Addition of equation 2.2 and 2.3 cancels all odd order terms and leaves

$$r(t + \Delta t) = 2r(t) - r(t - \Delta t) + \ddot{r}\Delta t^2 + O(\Delta t^4) \qquad (2.4)$$

Equation 2.4 is an example of the working equation necessary to perform a molecular dynamics simulation using the Verlet algorithm. In actual use, velocities are also

computed and used in conjunction with equation 2.4, but for our illustrative purpose, the form of equation 2.4 is sufficient.

According to equation 2.4, the particle positions at time $(t + \Delta t)$ can be obtained from knowledge of the positions at the current time t, positions at time $(t - \Delta t)$, and the accelerations (term involving the second time derivative). The only sources of error in equation 2.4 and the resulting phase space trajectories which would result from use of this particular algorithm are the intrinsic instability of the finite difference approach, the necessary truncation of the Taylor series' (equations 2.2 and 2.3), and the accelerations which enter equation 2.4. The discretization error can be controlled with the use of small time steps, Δt, in the numerical integration of the equations of motion. In addition, the truncation error of the formally infinite Taylor series, as shown in equation 2.4, is fourth order in Δt. Provided that the time step, Δt, is chosen to be small, this truncation error will become infinitesimal. In practice, time steps on the order of femtoseconds are used; therefore the truncation error can be safely disregarded in the determination of the trajectories via equation 2.4. The appropriateness of a chosen time step can be tested by running a simulation and comparing the results to a simulation where a smaller time step is used. If there is no appreciable change in the results then an appropriate choice has been made for the time step.

Given that the truncation error is negligible, the only remaining source of error in equation 2.4 is due to the accelerations. The accelerations are evaluated according to equation 2.1 (Newton's equation of motion). Examination of equation 2.1 shows that the computed accelerations are directly contingent upon the potential used to model the interaction among the particles. Therefore, in order for the phase space trajectories which

result from a simulation to be indisputable, knowledge of an exact, or at least chemically accurate, potential is required. Given such a potential, which must result from a quantum mechanical treatment, there would be no formal source of error (other than numerical precision) inherent in the molecular dynamics simulation. A simulation of this quality is considered to be "predictive".

Molecular Dynamics Potentials

Classical Potentials

> One solution to this problem is to construct an empirical interatomic potential, which gives the energy E of a set of particles, as an explicit mathematical function of the set of particle coordinates. If this function is sufficiently easy to calculate, and if it gives a sufficiently accurate description of the real physical system of interest, then one can perform realistic calculations of the properties of quite large systems. . . .Of course, such an approach will inevitably involve a significant loss of accuracy, compared with *ab initio* calculations. – [8, p. 6991]

Though the need for *ab initio* quantum mechanical potentials is recognized, the choice of empirical potential becomes a computational necessity as the evaluation of the forces of interaction using an *ab initio* wavefunction technique, for systems with more than a few hundred atoms, is mostly impossible using modern computers. For systems whose size *is* amenable to *ab initio* treatment, the computation is still too time consuming to be practical for routine application in molecular dynamics where several thousand time steps, each of which requires an evaluation of the wavefunction, may be necessary in order to observe the phenomena of interest. Therefore, in practice, most molecular dynamics simulations employ parameterizable potentials of relatively simple form to determine the variation of the particle positions with time. Although these potentials can be rapidly evaluated and are applicable to much larger scale systems than possible with *ab initio* techniques, they are in error in comparison to results obtained from first

principles quantum mechanics computations on small clusters; thus they can not be considered predictive. Furthermore, classical potentials can not distinguish between radicals and ions, different spectroscopic states, or be used to properly describe bond breaking in molecules.

Two body potentials

There are many parameterizable classical pair potentials available for use in simulations, each designed to suit the problem of interest. Once a choice of functional form has been made for the potential, the parameters are fit to be descriptive of the system to which the potential will be applied. As an example, consider the classical pair potentials of van Beest *et al.* (BKS) [9] and Tsuneyuki *et al.* (TTAM) [10] which were designed to be applicable to large polymorphs of silica. The BKS and TTAM potentials are very similar and have the functional form

$$V(r) = \sum_{i \neq j} \frac{q_i q_j}{r_{ij}} + a_{ij} \exp(-b_{ij} r_{ij}) - \frac{c_{ij}}{r_{ij}^6} \qquad (2.5)$$

where the first term models the Coulomb charge-charge interaction between particles of charge q. The remaining two terms are collectively called the "Buckingham term" and are intended to model the short-range repulsive and dispersion interactions [11]. This potential consists of 11 parameters consisting of the charges on silicon and oxygen, and the three pair parameters a_{ij}, b_{ij}, and c_{ij} for each pair interaction (O-O,Si-Si,Si-O).

To determine the parameters, guided by the low pressure crystal structure of silica which is composed of corner sharing SiO_4 tetrahedra, the BKS and TTAM potentials were fit to reproduce the *ab initio* Hartree-Fock potential energy surfaces of SiO_4H_4 and $SiO_4(4-) + 4\epsilon^+$ clusters respectively. The BKS parameterization was further augmented with experimental data for the elastic constants and unit-cell dimensions of quartz. The

Hartree-Fock potential energy surface of the SiO_4 cluster was that corresponding to T_d and D_{2h} distortions of the oxygen atoms from their equilibrium positions. Examination of figures in the original TTAM paper indicate that the *ab initio* potential was sampled in the region of $R_{eq} - 0.2$ to $R_{eq} + 0.4$ Angstroms and that the chosen functional form of the pair potential reproduces the shape of the *ab initio* potential energy surface in that region.

Examination of the BKS/TTAM parameterization is a clear example of the seemingly arbitrary parameter choice evident in some pair potentials. The assignment of the silicon and oxygen charges (+2.4 and –1.2 respectively) by BKS and TTAM were based on Mulliken population analyses of the SiO_4 parameterization cluster [12]. It is well known that Mulliken population analyses are very much dependent on choice of basis set and may not be a reliable indication of atomic charge and a better choice would have been a charge analysis based on the use of natural atomic orbitals which are contingent upon the electron density and not the basis set, though some effect will still be evident [13-14].

Further, the *ab initio* surface was only explored in regions close to equilibrium with low level Hartree-Fock calculations. Although Hartree-Fock theory gives equilibrium geometries which are in good agreement with experiment, the BKS and TTAM potentials have been used extensively to study *fracture* in bulk silica [15-16]. Fracture entails the breaking of chemical bonds and sampling of configurations far from equilibrium. Therefore, a classical potential, which derives from only near equilibrium reference data, has to be used with caution when applied to non equilibrium phenomena such as fracture. The inability of the BKS/TTAM potential form to break chemical bonds is clearly demonstrated in Figure 2-1 where the potential energy surface for rupture of a

brigded Si-O bond (see figure) in pyrosilicic acid ($Si_2O_7H_6$) at the *ab initio* coupled cluster level of theory (CCSD with a DZP basis) is compared to that obtained with the BKS potential. The CCSD model has a demonstrated ability to achieve chemical accuracy [17] however; the BKS potential grossly underestimates the dissociation energy which results from the quantum calculation and is also in error in the repulsive region.

Also shown is a plot of the forces which result from the computed potential energy surface. These forces are those which would be used in a molecular dynamics simulation and the classical forces are clearly in error in comparison to the quantum mechanical forces in both the repulsive and bond break regions. Given that the classical potential does not reproduce the *ab initio* results, any molecular dynamics simulation based on these potentials cannot be considered predictive.

Three body potentials

A natural first step in improving the performance of pair potentials is to evaluate interactions which involve atomic triples in conjunction with effects from atomic pairs. Potentials of this type are crucial to the proper description of covalently bonded materials which present a difficult challenge for classical potentials because complex quantum effects, such as hybridization and charge transfer, have to be described by an effective interaction in which the quantum mechanical degrees of freedom have, in some way, been integrated out [18]. Further, general pair potentials favor the formation of close-packed structures, whereas most covalently bound systems, such as silicon, have more *open* structures and require a proper description of three particle interactions [19].

As an example, consider the three body potential of Stillinger and Weber [20]. This potential has been used extensively in the study of bulk silicon and consists of a two

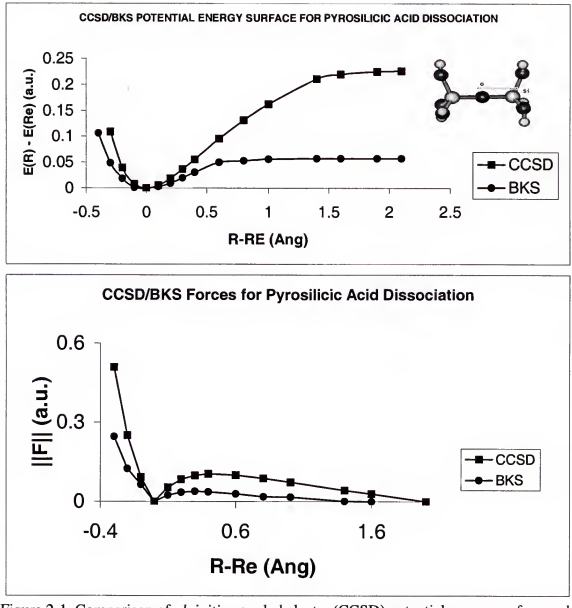

Figure 2-1. Comparison of *ab initio* coupled cluster (CCSD) potential energy surface and associated forces versus those obtained with the classical BKS pair potential for pyrosilicic acid dissociation. The reactive bond is indicated in the figure.

body contribution, and a three body term, V_3, expressed as a separable product of radial functions g(r) and an angular function

$$V_3(r_{ij}, r_{ik}) = g(r_{ij})g(r_{ik})(\cos\Theta_{jik} - \frac{1}{3})^2 \qquad (2.6)$$

where Θ_{jik} is the angle subtended by atoms j and k at the vertex i. The V_3 term has a minimum at Θ=109.5°; thus the potential discriminates in favor of tetrahedral bond angles which are prominent in the most stable zero temperature and pressure configuration of silicon, the diamond lattice [21].

In addition to the structure of the diamond lattice, the SW potential was parameterized such that the melting point and the liquid structure of the resulting melt was in agreement with experiment. Although the equilibrium properties of silicon were well characterized with the SW potential, a study conducted by Dodson [22] on the growth of silicon by the addition of layers only a few atoms thick showed that the potential was inadequate in regions away from the ideal geometry and where the sp^3 hybridization of the equilibrium configuration had been destroyed. Similar conclusions concerning the failure of the SW potential must apply to fracture as well, where non ideal local geometries will certainly occur.

Conclusions analogous to those of Dodson were reported by Biswas and Hamann [23] and led to the formulation of a new family of three body potentials by Tersoff [24]. These three body potentials are fundamentally different from those of Stillinger and Weber in that the strength of individual bonds is contingent upon the local environment and they are not implicitly biased to favor tetrahedral bond angles. Andreoni and Pastore [25], also motivated by the growth process of silicon, studied the applicability of the Tersoff potential to small silicon clusters that exhibit geometries which differ from the local equilibrium configurations of bulk silicon. In this work, the geometries and relative energetics of Si_N (N=4-10) clusters resulting from the Tersoff potential were compared to first principles density functional theory calculations The results showed that the

geometric topology of the N=4,8-10 clusters were predicted incorrectly by the Tersoff potential and that the energy ordering of different local minima was not in accord with the *ab initio* potential.

As a final example of the failure of the three body potential form when compared to *ab initio* calculations, consider the potential of Vashishta *et al.* [26] which was parameterized for study of amorphous silica. This potential consists of a two body part which includes terms to model the steric repulsion of ions of different size, long range Coulomb interaction, and a charge-dipole interaction to model effects due to polarization of anions. The three body function is a separable product of a radial function and an angular term, scaled by a strength parameter which is contingent upon the angle (Si-O-Si or O-Si-O) type. The three body term, similar to that of Stillinger and Weber, is biased towards angles which correspond to those observed at equilibrium. The parameters in the potential were taken from standard tables (polarizability of oxygen), empirically chosen based on the authors' experience, and some were numerically fit to reproduce the experimental melting temperature and pressure of silica.

A comparison of the potential energy surface and associated forces for the *ab initio* and classical 3-body potential of Vashishta *et. al* is shown in Figure 2-2. Although the three body potential includes higher order interactions than do the pair potentials, the agreement with the *ab initio* results is still poor.

Quantum Potentials

High level *ab initio* molecular orbital calculations are an ideal choice of potential for use in molecular dynamics simulations. *Ab initio* techniques are capable of properly characterizing the geometric and energetic topology of systems both near and far from equilibrium which, thus far, has not been possible with classical potentials. Further,

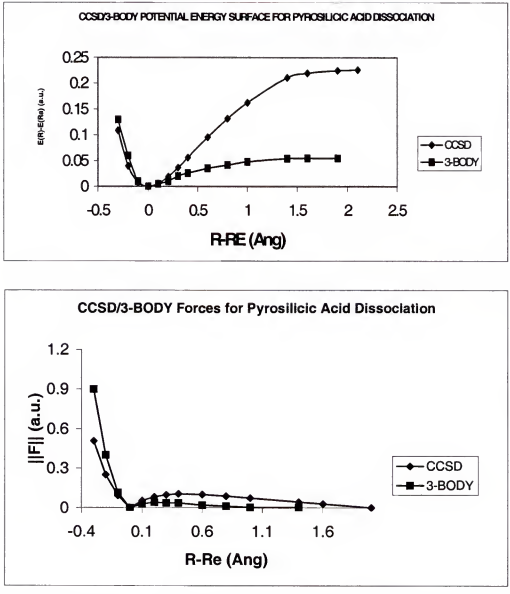

Figure 2-2. Comparison of *ab initio* coupled cluster (CCSD) potential energy surface and associated forces versus those obtained with the 3-body potential for pyrosilicic acid dissociation. The reactive bond is shown in Figure 2-1.

quantum mechanical potentials are able to distinguish among different states which is not even a concept when dealing with classical potentials. This type of flexibility is necessary when dealing with non-equilibrium phenomena such as fracture where a variety of dissociation pathways are possible and need proper treatment. Although quantum mechanical potentials have some very attractive features, their applicability to

large scale simulation is severely limited by the computational cost of the methods. Due to this large computational scaling, quantum mechanical Hamiltonians used in simulations have been limited to density functional and semi-empirical forms.

Density functional potentials

The most rigorous quantum mechanical potentials routinely used in molecular dynamics simulations are those based on density functional theory (DFT) [27]. Although density functional methods give accurate geometries and forces, the system size (on the order of 100's of atoms) and time scale for simulations (a few picoseconds), is limited by the use of these potentials.

Semiempirical potentials – Tight binding and NDDO models

Due to the computational limitations of density functional potentials, semi-empirical quantum mechanical Hamiltonians, which encompass tight binding and the neglect of diatomic differential overlap (NDDO) models, have been used extensively in molecular dynamics simulations. In these schemes, the computationally expensive integrals present in *ab initio* methods are replaced by simple parametric forms.

There are many tight binding models available in the literature and they can be viewed as reparameterized Huckel methods which include short range repulsive terms [28]. The most commonly used and computationally simple forms assume an orthogonal basis where each atomic center is associated with a minimal set of valence atomic orbitals. The tight binding Hamiltonian (H_{TB}) is limited to one and two center interactions whose values are computed in terms of simple, parameterizable functions [29-31].

In the orthogonal tight binding method, once the Hamiltonian matrix has been built, the one particle states are determined in a ***non*** self-consistent manner by solving

$$H_{TB}\Psi_i = \varepsilon_i \Psi_i \tag{2.7}$$

and the total energy is given by

$$E_{TOT} = \sum_{\text{occ i}} \omega_i \varepsilon_i + \sum_{i \neq j} V_{rep}(r_{ij}) \tag{2.8}$$

where ω_i is the orbital occupation number and the second term, V_{rep}, models the electrostatic repulsion between atomic cores [31]. Classically, this term is given as $Z_A Z_B / R_{AB}$; however, in tight binding models, this term is also treated as a parameterizable function.

The ***non*** self-consistent nature of the tight binding method, combined with the simplicity of the Hamiltonian matrix elements, renders tight binding faster and applicable to larger size systems than first principles techniques. In self-consistent methods (i.e., Hartree-Fock) where the Hamiltonian depends upon the electron density, repeated diagonalizations, which scale cubically with the size of the basis set, are required. This is often the rate-determining step in the computation. However, the tight binding Hamiltonian does not depend on the electron density; therefore the one particle states are obtained after a *single* matrix diagonalization. Although the non self-consistent nature of the tight binding Hamiltonian is advantageous in regard to computational speed, it suffers a serious deficiency in that system charge is ignored [29]. Computationally, the tight binding Hamiltonian predicts the same eigenvalues and eigenvectors, irrespective of the number of electrons in the system. As a result of this, the only quantity which distinguishes states of a different charge is the total energy which is contingent upon the orbital occupation numbers (see equation 2.8). However, since tight binding predicts the same orbital energies for all charge states, the total energy (and associated forces)

computed via equation 2.8 must be in error since adding or removing particles changes the Coulomb interactions among the electrons and will cause a shift in the eigenvalue spectrum.

Given the wide variety of tight binding parameterizations available in the literature, it is difficult to generalize the success of the method when compared to *ab initio* results. Panda *et al.* [30] did a comparison of DFT and *ab initio* Hartree-Fock theory to the orthogonal tight binding parameterizations of Kwon *et al.* [32] and Lenosky *et al.* [33]. In this work, a comparison of binding energies, equilibrium geometries and dipole moments was made for small Si_N clusters up to N=19. For the binding energies, it was reported that the parameterization of Kwon *et al.* agreed with the Hartree-Fock results for clusters up through N=10; however, the Lenosky *et al.* parameterization predicted binding energies which were too low. Geometrically, the tight binding models used in this work gave errors in bond lengths of ≈0.2 Angstroms in comparison to the density functional geometries and in some cases tight binding predicted a different geometric topology (D_{3h} versus C_{3v}) than did the density functional method. Overall, the agreement with *ab initio* results for these models is fair but, unfortunately, this study and work similar to it done by other researchers using different tight binding parameterizations, do not sample non-equilibrium configurations. Similar to the situation with classical potentials, tight binding has been used extensively to study fracture where non-ideal geometries will occur. However, the fidelity of the method at configurations away from ideality has not been well reported. There have been some studies of defect sites (removal of an atom) in bulk silicon [31], but these studies are focused primarily on

energetic effects and not the local geometry at the defect, which is indicative of forces, the determining factor for a predictive simulation.

In addition to tight binding models, semi-empirical Hamiltonians based on the neglect of diatomic differential overlap (NDDO) approximation have been used to generate forces in molecular dynamics simulations [34]. The NDDO based methods are, similar to tight binding methods, parameterizable Hamiltonians limited to two center interactions at most, where the Coulombic repulsion between atomic cores is included in an ad hoc way (i.e., not $Z_A Z_B / R_{AB}$). However, the NDDO methods are a step towards *ab initio* theory because non-zero one and two electron integrals are computed explicitly in terms of parameterizable functional forms [35].

Computationally, NDDO methods are single determinant, self-consistent, Hartree-Fock level calculations, where the elements of the Fock matrix are built from parameterized integrals. Although electron correlation may be considered explicitly, typically via configuration interaction, it is generally regarded that NDDO models include correlation at the Hartree-Fock level via inclusion of parameterized integrals which are fit to experimental or correlated *ab initio* results [36]. Therefore, since correlation is included implicity in the parameterization, to avoid any possible "double-counting" of correlation corrections, most NDDO results are reported at the Hartree-Fock level. The self-consistent nature of the NDDO Hamiltonian renders it applicable to both open and closed shell systems which is a distinct advantage over the tight binding models. However, because of the requisite matrix diagonalizations necessary to achieve self-consistency of the density and the computation of two electron integrals included in

the model, the NDDO methods are an order of magnitude slower than tight binding formulations in regard to computational speed.

There are many parameterizations of the NDDO Hamiltonians available for routine use [37]. Although NDDO methods are used to study many properties such as ionization potentials, heats of formation, and dipole moments, the ability to predict accurate geometries is most important for molecular dynamics because accurate geometries indicate an accurate treatment of forces. For ground state equilibrium geometries, all methods perform well with average errors in bond lengths and angles of ≈0.05 Angstroms and 4° respectively as compared to experiment, but there are some cases where the methods produce much larger than average errors [35].

Although the NDDO methods are attractive models for use in molecular dynamics simulations they, similar to other classes of potentials, are parameterized to reproduce equilibrium properties. Therefore, the potential energy surface in regions away from equilibrium cannot be expected to be well characterized with these models. As a demonstration of the failure of the NDDO potentials at non equilibrium configurations, consider Figure 2-3 which compares results from *ab initio* CCSD calculations to those of two existing NDDO Hamiltonians, AM1 and MNDO/d. There it is demonstrated, most notably for the forces, that the NDDO Hamiltonians fail to accurately describe pyrosilicic acid in regions away from equilibrium.

Conclusion

This chapter introduced the term "predictive simulation" and demonstrated the lack of accuracy, as compared to *ab initio* theory, for some of the commonly used classical and quantum potentials. Given the demonstrated necessity of accurate, rapidly

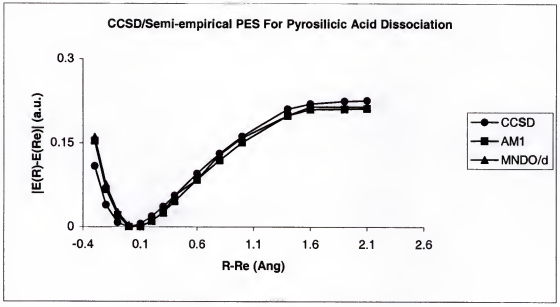

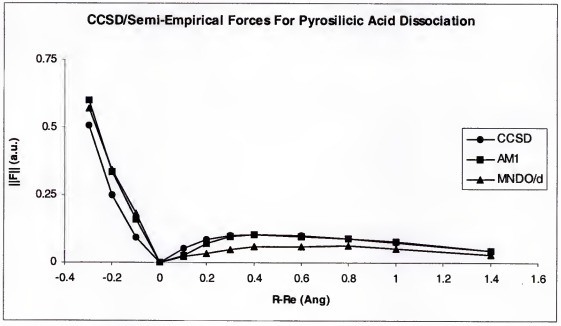

Figure 2-3. Comparison of *ab initio* coupled cluster (CCSD) potential energy surface and associated forces versus those obtained with the semi-empirical AM1 and MNDO/d potentials for pyrosilicic acid dissociation. The reactive bond is shown in Figure 2-1.

calculable potentials for molecular dynamics, the concept of the transfer Hamiltonian is introduced in the following chapter. It will be seen that the transfer Hamiltonian is a parameterizable quantum mechanical operator designed to accurately reproduce *ab initio*

forces, the most important quantity for accurate simulations, yet the computational scaling is much lower than first principles calculations. The transfer Hamiltonian will be shown to be a practical tool for molecular dynamics simulation.

CHAPTER 3
TRANSFER HAMILTONIAN

Introduction

This chapter will present two formal justifications of the transfer Hamiltonian in terms of coupled cluster theory and from a density functional viewpoint. It will be seen that the transfer Hamiltonian can be viewed as approximations to either of these models which, in principle, provide *ab initio* analogs to the parameters which comprise the semi-empirical transfer Hamiltonian. Following the more formal arguments, the functional form of the transfer Hamiltonian will be presented in detail.

Theoretical Formulation

It has been shown that both classical and semi-empirical potential forms (in their standard formulations) are inadequate when non-equilibrium areas of the potential energy surface are sampled. In simulations of fracture, where bonds are being broken, it is necessary to have a quantum mechanical potential which is capable of accurately treating both equilibrium and non ideal configurations if the simulation is to be considered predictive. However, the potential must be rapidly calculable and applicable to systems large enough to properly simulate the phenomena of interest.

As a means to this end, the concept of the transfer Hamiltonian is introduced. The transfer Hamiltonian is a low rank, self-consistent, quantum mechanical operator whose matrix elements are given in terms of parameterizable functions. The functional form of the transfer Hamiltonian may be chosen freely; however the existing NDDO

Hamiltonians are a judicious choice due to their demonstrated ability to reproduce *ab initio* geometries in equilibrium regions. In general, once a choice of functional form has been made, the parameters of the transfer Hamiltonian are fit using numerical optimization algorithms such that the forces and other quantities of interest given by the transfer Hamiltonian reproduce those given by *ab initio* theory.

The transfer Hamiltonian, constructed in this way, is a useful tool for molecular dynamics simulations because it provides a convenient route for the predictive simulation of materials without the computational bottleneck of *ab initio* potentials. Further, the transfer Hamiltonian is superior to classical potentials and tight binding models due to its demonstrated ability to properly describe different charge states and a wide range of geometric topologies.

The functional form of the transfer Hamiltonian may be chosen freely, however, practitioners of semi-empirical quantum chemistry, in its NDDO formulation, have developed a variety of approximate Hamiltonians which are used here as models though some variations are made from the standard representations. Operationally, the transfer Hamiltonian calculation is simply an independent particle, self-consistent field computation based on a single determinant reference. However, due to the parameterization, the energies and forces are formally exact. This type of structure is similar to that of density functional theory where the energies and associated forces are exact although the effective Hamiltonian used in the model is of one-particle type [38]. The formal analysis of the transfer Hamiltonian can be presented in terms of coupled cluster or density functional theory, both of which, in principle, are *ab initio* representations of the transfer Hamiltonian.

Coupled Cluster Theory Formulation

In coupled cluster theory, the ground state wavefunction is given by

$$\left|\Psi_g\right\rangle = e^T \left|\phi_o\right\rangle \tag{3.1}$$

where ϕ_o is a single Slater determinant and T is an excitation operator which creates single, double, up to n-tuply excited configurations from the reference determinant. T can be written as

$$T = T_1 + T_2 + \ldots = \sum_{i,a} t_i^a a^+ i + \frac{1}{2} \sum_{i,j,a,b} t_{ij}^{ab} a^+ i b^+ j + \ldots \tag{3.2}$$

where the standard creation/annihilation operators have been used [39]. A coupled cluster calculation reduces to a determination of the t amplitudes present in each level of excitation and, as equation 3.2 shows, it is not based on an independent particle treatment of the electrons as is the transfer Hamiltonian.

The connection of the independent particle transfer Hamiltonian to many body coupled cluster theory can be made via consideration of the effective one-particle Hamiltonian which arises in Brueckner–Coupled Cluster (BCC) theory [40]. The Brueckner model is a version of coupled cluster theory where the orbitals are optimized so that the single excitation amplitudes are equal to zero (T_1=0 in equation 3.2) In BCC, the total energy is the sum of the independent particle reference determinant energy and a correlation term:

$$E = \left\langle \Phi \left| e^{-T} H e^T \right| \Phi \right\rangle = E_{ref} + E_{corr} \tag{3.3}$$

$$E_{ref} = \frac{1}{2} \sum_i (h_{ii} + f_{ii}) \tag{3.4}$$

$$E_{corr} = \frac{1}{4} \sum_{ijab} t_{ij}^{ab} \left\langle ab \middle\| ij \right\rangle \tag{3.5}$$

where the equations have been written in the spin orbital basis and i,j (a,b) refer to occupied (virtual) spin orbitals. In the following, indices p,q denote orbitals in both occupied and virtual spaces. **h** is the one electron Hamiltonian which contains the kinetic energy and nuclear-electron attraction terms and the fock matrix elements **f** which appear in equation 3.4 are given by

$$f_{pq} = h_{pq} + \sum_{j} \langle pj \| qj \rangle \tag{3.6}$$

The total energy expression in equation 3.3 can be written in terms of an effective Hamiltonian, **G**:

$$E = \frac{1}{2} \sum_{i} (h_{ii} + G_{ii}) \tag{3.7}$$

where the general matrix element of the occupied-occupied block of **G** is given by

$$G_{ik} = f_{ik} + \frac{1}{2} \sum_{jab} \langle ab \| kj \rangle t_{ij}^{ab} \tag{3.8}$$

and the occupied-virtual block of the effective matrix is chosen to be the T_1 amplitude equation

$$T_1 \equiv G_{ia} = f_{ia} + \sum_{jb} f_{jb} t_{ij}^{ab} + \frac{1}{2} \sum_{jbc} \langle bc \| aj \rangle t_{ij}^{bc} - \frac{1}{2} \sum_{jkb} \langle ib \| jk \rangle t_{jk}^{ab} \tag{3.9}$$

Solution of the set of one-particle like equations

$$G \phi_i = \varepsilon_i \phi_i \tag{3.10}$$

yields a set of orbitals (Brueckner orbitals) which satisfy T_1=G_{ia}=0 i.e the Brueckner condition. These orbitals are then used to generate a new set of T amplitudes which define a new effective operator and the procedure is repeated until self-consistency is

achieved. The effective matrix **G** and the T amplitude equation are solved repeatedly until the T amplitudes, and consequently the **G** matrix, do not change in successive iterations.

The total energy expressed in terms of the effective one-particle operator **G** (see 3.7), is equivalent in form to that of the independent particle Hartree-Fock model (compare equations 3.4 and 3.7) and it can be concluded that BCC is an effective one-particle theory whose energy and associated forces are exact.

When viewed in this way, the transfer Hamiltonian, T_h, can be considered as an approximation to **G** since both operators yield energies and forces which are formally exact. In the Brueckner-coupled cluster case, the correlation contribution to **G** is included via an iterative determination of the T_2 amplitudes which determine the matrix elements of the effective one-particle operator **G**. However, in the T_h case, the many body contribution to the energies/forces is obtained via parameterization of the matrix elements. Since each operator involves correlation corrected matrix elements which yield the exact energy and forces, **G** serves as an *ab initio* analog of the semi-empirical operator T_h.

Similar approaches have been considered by Karl Freed [41] and coworkers who attempt to compute semi-empirical PPP Hamiltonian parameters from first principles. In their approach, they consider the matrix equation

$$\begin{bmatrix} PHP & PHQ \\ QHP & QHQ \end{bmatrix} \begin{bmatrix} P\Psi \\ Q\Psi \end{bmatrix} = E \begin{bmatrix} P\Psi \\ Q\Psi \end{bmatrix} \qquad (3.11)$$

where P is the primary space and Q is the orthogonal complement to P. Simple algebraic manipulations starting from equation 3.11 yield an effective Hamiltonian

$$H_v = PHP + PHQ\,(E - QHQ)^{-1} QHP \qquad (3.12)$$

where H_v acts only in the primary space but yields the exact energy E [42-43]. If the primary space is considered to be a ground state single determinant reference and the orthogonal complement Q includes all single, double, to n-tuply excited determinants, then, similar to the coupled cluster case (**G**), H_v consists of correlation corrected integrals which are *ab initio* analogs of semi-empirical parameters.

The coupled cluster viewpoint is a more convenient and transparent route to an *ab initio* representation of the semi-empirical Hamiltonians since it bypasses the energy dependence and large matrix inversion required in the H_v approach. In practice, the inverse matrix is replaced by a perturbation expansion and the equation solved iteratively [41]. On the contrary, the representation of the matrix elements of **G** are given by closed formulas in terms of many body integrals and **T** amplitudes determined in the coupled cluster calculation [40]. Further, for a given choice of Q space determinants, coupled cluster theory will include contributions due to higher excitation manifolds than the H_v approach due to the exponential form of the wave operator used in coupled cluster theory [39]; therefore the correlation corrected integrals of **G** will contain more of the inter-electron physics and provide a better estimation of the semi-empirical parameters than those of H_v.

Density Functional Theory Formulation

Density functional theory is an exact one-particle theory where it is possible, in principle, to solve for the exact energy (including electron correlation) through the treatment of a set of one particle equations [38]. The density functional energy can be written as

$$E_{DFT}[\rho] = E_{KE} + E_{Ne}[\rho] + E_{J}[\rho] + E_{XC}[\rho] \qquad (3.13)$$

where the final term, the exchange-correlation energy, includes the stabilizing effects of electron exchange (**K** operator in Hartree-Fock theory) and correlation into a single functional of the density. Given an exact exchange-correlation energy functional, E_{DFT} would be the exact energy although the method is of one-particle type, analogous to the transfer Hamiltonian.

The functional derivative of the exchange-correlation energy functional yields the exchange-correlation potential. This potential, when combined with the usual expressions for the one electron core Hamiltonian and two electron coulomb integrals (J) yields an effective one-particle operator **G** such that

$$G\,\phi_i = \varepsilon_i \phi_i \qquad (3.14)$$

The resulting one-particle functions {ϕ} yield a density, which when evaluated in equation 3.13, render an energy and forces which are formally exact. The exchange-correlation functional, similar to the role of the parameters contained in the transfer Hamiltonian, yields an effective operator that is of one-particle type yet yields exact energies and forces, therefore, the transfer Hamiltonian can be interpreted as modeling the Kohn-Sham operator.

Strictly speaking, in order to proceed with this interpretation, the transfer Hamiltonian matrix elements should be computed using the exchange-correlation potential (or some approximation to it) used to solve the first principles Kohn-Sham equations. However, the DFT based transfer Hamiltonian is treated via a HF-DFT (Hartree-Fock DFT) computation where the general exchange-correlation functionals are

applied to the converged transfer Hamiltonian density determined at the Hartree-Fock level [44]. When treated in this way, the parameters which comprise the transfer Hamiltonian cannot be interpreted as modeling correlation corrections as in the coupled cluster case because the correlation contribution to the energy is taken care of by the exchange-correlation functional. The parameters, in the context of a transfer Hamiltonian based on HF-DFT, are simply approximations to the *ab initio* one and two-electron integrals.

In summary, the transfer Hamiltonian is an effective one particle operator which yields exact energies and forces by virtue of parameters. This operator is similar to the effective one-particle operator which arises in Brueckner coupled cluster theory or the Kohn-Sham operator of density functional theory, both of which provide *ab initio* representations of the transfer Hamiltonian.

Functional Form

Given a coupled cluster or DFT based transfer Hamiltonian, the parameterizable one and two electron integrals over atomic basis functions have to be computed in a suitable fashion and the Hartree-Fock self consistent field equations solved. In *ab initio* models, these integrals are almost universally computed using gaussian type basis functions for which the requisite poly-centric integrals can be computed analytically [45]. However, for the transfer Hamiltonian, these integrals are determined in terms of parameterizable functions.

The chosen integral approximations in the coupled cluster or density functional variant of the transfer Hamiltonian, are taken from the established field of semi-empirical theory in its modified neglect of differential overlap (MNDO) formulation [46].

In MNDO, the zero differential overlap approximation,

$$f[\phi_{\mu}^{A}(1), \phi_{\nu}^{B}(1)] = \delta_{AB} f[\phi_{\mu}(1), \phi_{\nu}(1)] \qquad (3.15)$$

is invoked where Φ_μ and Φ_ν are basis functions on centers A and B respectively. The implication of equation 3.15 is that all integrals which involve multi-center charge distributions are zero which limits the Hamiltonian to two-center interactions at most.

MNDO assigns to each atom a set of *valence*, Slater atomic orbital basis functions [47]. Therefore, each first/second row atom receives a set of sp Slater basis functions (for a total of 4) and all higher row atoms receive a set of spd (9) orbitals. In some cases, a set of polarization functions may be used for hydrogen and the first/second row atoms. In that case, hydrogen is assigned an additional set of p orbitals and the first/second row atoms are associated with a set of spherical harmonic d functions.

MNDO is a valence electron model, therefore the effective nuclear charge for each atom is given by Z'=Z-n where n is the number of core electrons for the atom. Given the basis set and nuclear charges, the one and two electron integrals are computed parametrically as follows [35]:

(in the following equations (μ,ν) and (κ,λ) are basis functions assigned to centers A and B respectively)

One Center – One Electron Integrals

For basis functions μ and ν on atomic center A, the one electron integrals are given by

$$H_{\mu\mu} = U_{\mu\mu} - \sum_{A \neq B} Z_B (\mu\mu \mid s_B s_B) \qquad (3.16)$$

for the diagonal elements and

$$H_{\mu\nu} = -\sum_{A \neq B} Z_B (\mu\nu \mid s_B s_B) \qquad (3.17)$$

for the off diagonal contributions. $U_{\mu\mu}$ in equation 3.16 is treated as a parameter and is interpreted as the one center atomic orbital energy of the μ'th orbital (μ=s,p,d orbital). This parameter can be taken from atomic spectral data or varied in the parameterization of the transfer Hamiltonian. If the latter is chosen, care must be taken to ensure that the U parameters for each atom have the proper energy ordering. In other words, the U parameter for an s type basis function should be more negative than that for p and so on. This is consistent with the interpretation that U models the one center atomic orbital energy and the work required to remove an electron from an s orbital is greater than that for a p orbital and similarly for the d orbital.

As equations 3.16 and 3.17 show, the attraction of an electron with charge distribution centered on atom A for a nucleus B is modeled in terms of the effective nuclear charge of center B, weighted by the two-electron repulsion integral involving the charge distribution of center A and the spherically symmetric distribution |ss) of center B. This formula was determined empirically, without theoretical justification [48].

Two Center – One Electron Integrals

Although the ZDO approximation implies that this class of integrals is zero, they are retained in the model because it was found, by the early practitioners of semi-empirical methods, that bonding between atoms was much improved by their presence in the model [36]. For a two center charge distribution μ on A and κ on B, the two center core Hamiltonian matrix element is computed as

$$H_{\mu\kappa} = \frac{1}{2}(\beta_\mu + \beta_\kappa) S_{\mu\kappa} \qquad (3.18)$$

where $S_{\mu\kappa}$ is the overlap integral between the two basis functions. β is a freely variable atomic parameter with a separate value for each basis function type (s,p,d) assigned to each center. The value of this matrix element is also contingent upon the Slater orbital exponent which determines the value of the overlap integral. The orbital exponents are also considered to be variable parameters.

One Center – Two Electron Repulsion Integrals

The one center, two electron repulsion integrals are treated differently depending on the type of basis functions assigned to each center [48]. For an atom with an sp basis set, there are only 6 two electron repulsion integrals which are non-zero by symmetry. The six integrals, are given by:

$$\begin{aligned} G_{ss} &= (s\ s \mid s\ s) & G_{sp} &= (s\ s \mid p\ p) \\ G_{pp} &= (p\ p \mid p\ p) & H_{sp} &= (s\ p \mid s\ p) \\ G_{p2} &= (p\ p \mid p'\ p') & H_{pp} &= (p\ p' \mid p\ p') \end{aligned} \qquad (3.19)$$

For an sp basis set, due to the small number of integrals and to add more flexibility to the parameterization, these integrals are treated as variable parameters. On the contrary, for a basis set which includes d orbitals, due to the large number of non-zero integrals, all the one center two electron repulsion integrals are computed analytically in terms of Slater-Condon F/G factors [49]. These integrals are computed with an additional set of orbital exponents which differ from the orbital exponents used to compute the overlap integrals that determine the two-center core Hamiltonian matrix elements.

Two-Center Two Electron Repulsion Integrals

Due to the ZDO approximation, all three and four center two electron repulsion integrals are neglected. The two center integrals which remain are treated by the point charge model of Thiel and Dewar [50]. In this model, the one center charge

distributions on each center are expanded in terms of multipoles and each multipole is then represented by an appropriate point charge configuration centered on each nucleus. Finally, the interaction of each point charge of center A with those of B is evaluated using the Ohno-Klopman formula and summed to give the two electron repulsion integral [51].

The value of this class of integrals is parameterized in terms of the orbital exponents assigned to each nucleus. The orbital exponents determine the distance of each point charge from its respective nucleus. Therefore, diffuse orbital exponents render point charge configurations which are greater distances from each nucleus and yields larger values of the two center repulsion integrals. This is similar to *ab initio* models where diffuse orbitals have a larger radial extent and yield larger integral values [52].

In addition to the orbital exponents, the two-center repulsion integrals also depend on the value of the one center repulsion integrals which may also be parameters as described previously. The Ohno-Klopman formula which is used to evaluate the interaction between point charges i and j is given by

$$e^2 [R_{ij}^2 + (\rho_o^A + \rho_o^B)^2]^{\frac{-1}{2}} \qquad (3.20)$$

where R_{ij} is the separation between the point charges. The additive terms ρ^A and ρ^B are constants assigned to each atom which are determined such that the value of the corresponding one center two electron repulsion integral is reproduced in the limit $R_{ij}=0$. Computationally, once the one-center integrals are determined, the equations which determine the additive terms ρ^A and ρ^B are solved numerically for each atom as an analytic solution is only possible for the one center (ss|ss) repulsion integral [50].

Given the point charge separations and the additive terms which enter the Ohno-Klopman formula for each nucleus, the two electron integrals can be rapidly evaluated. Due to the large number of these integrals (i.e. 2025 integrals for two atoms with spd basis sets), they are computed in a local coordinate system where symmetry reduces the number of non-zero integrals which need be evaluated. The resulting symmetry integrals in the local frame are subsequently transformed into integrals over molecular coordinates using p and d orbital rotation matrices [53].

Nuclear Repulsion Energy

In *ab initio* theory, the nuclear repulsion between two atomic cores is given by $Z_A Z_B / R_{AB}$, however, in the MNDO model this term is represented by a parameterizable function. The core-core repulsion energy is given by

$$E(A,B) = Z_A' Z_B' (s_A s_A \mid s_B s_B)(1 + e^{-\alpha_A R_{AB}} + e^{-\alpha_B R_{AB}}) + \sum_i a_{i,A} e^{-b_{i,A}(c_{i,A} - R_{AB})^2} + a_{i,B} e^{-b_{i,B}(c_{i,B} - R_{AB})^2} \qquad 3.21$$

where the α exponents of the lead term, and the (a,b,c) parameters of the second term are variable parameters.

Computational Procedure

The transfer Hamiltonian is merely a parameterized Hartree-Fock computation where the parameterization is in terms of the integrals over the basis functions and the internuclear repulsion energy expression, as presented in the previous sections. A summary of the available parameters is given in Table 3-1. The parameterized integrals are summed into matrix elements using the usual equations from Hartree-Fock theory and the total energy and density are determined self-consistently. In the density functional based transfer Hamiltonian, the converged density is used to evaluate the chosen

exchange-correlation functional, otherwise, the electronic energy is computed as in Hartree-Fock theory via .5*Tr(P[H+F]) . P is the one-particle density matrix and H/F have their usual meanings.

Table 3-1: Listing of the atomic parameters which define the transfer Hamiltonian

Parameter	Description
Uss,Upp,Udd	One center atomic orbital energies (eqn. 3.16)
Zs,Zp,Zd	Orbital exponent for overlap integrals and charge separations
Zsn,Zpn,Zdn	Orbital exponent for one center, two electron repulsion integrals (d orbital basis)
βs,βp,βd	Beta resonance parameter for core Hamiltonian matrix elements (eqn. 3.18)
Gss,Gsp,Gpp,Gp2,Hsp,Hpp,	One center two electron repulsion integrals - sp basis (eqn. 3.19)
α,a,b,c	Core repulsion energy parameters (eqn. 3.21)

Parameterization

The parameterization of the transfer Hamiltonian is of extreme importance as the accuracy of the model is contingent upon the parameters which are used to build the operator. In order for the parameterization to proceed, it is necessary to have a set of *ab initio* reference data which the transfer Hamiltonian should reproduce and an algorithm to determine the optimal set of parameters. The reference data can be any quantity which should be reproducible by the transfer Hamiltonian; however, in the context of molecular dynamics, the forces are the most important properties. The parameterization is certainly not limited to forces, as one can also fit ionization potentials, dipole moments, vibrational frequencies, activation barriers or the density itself. It should be clear that the larger the

target reference data set, the worse the transfer Hamiltonian will perform, numerically, for each property. This is more a consequence of the convergence of the chosen numerical fitting algorithm than an inherent limitation of the Hamiltonian. Therefore, it is recommended to focus on one or two types of reference quantities (i.e. energy and forces) for each parameterization. Given the reference data, the parameters are determined using a combination of genetic and Newton-Rapshon optimization algorithms.

Conclusion

This chapter presented the formal justification and the functional form of the transfer Hamiltonian. It was seen that the integral approximations are simple in form and through their parameterization, provide a convenient route for the introduction of *ab initio* forces into molecular dynamics simulations, provided the parameters can be determined. That task is discussed in the following chapter.

CHAPTER 4
EXAMPLE TRANSFER HAMILTONIANS

Introduction

This chapter will detail the parameterization of the transfer Hamiltonian. The performance of the optimization algorithms for this task will be discussed and converged parameter sets for two representative molecules, ethane and disilane, will be presented as a demonstration of the procedure and the accuracy of the model.

Parameterization Procedure

The parameters of the transfer Hamiltonian are determined using genetic and quasi-Newton optimization algorithms. The complexity of the transfer Hamiltonian lies not in the concept of the method but in the difficulty of the parameterization. It is often stated that parameterizing is an art, not a science. The transfer Hamiltonian certainly corroborates that statement.

Genetic Algorithms

Genetic algorithms (GA) are stochastic optimization methods which take their terminology and conceptual basis from evolutionary biology [54]. GAs are based on Darwin's theory of evolution where the strongest, most fit individuals survive and produce offspring which have the favorable characteristics of the parent generation. The idea is to have a population of individuals, each characterized by a set of genes. The most fit parent individuals are allowed to produce offspring by sexual reproduction, and new and improved generations are produced while those less fit individuals are removed

from the population. After many generations, a population of strong individuals will be created.

GAs are a computational manifestation of evolutionary biology. In the context of the transfer Hamiltonian, the population is composed of trial parameter sets p, which are used to compute the one and two electron repulsion integrals described in chapter 3. The fitness of each parameter set is determined by computing the error, f , between properties computed with the transfer Hamiltonian and *ab initio* reference data using the equation,

$$f(p) = \sum_i |\omega_i^{Th} - \omega_i^{Ref}| \qquad (4.1)$$

where f(p) implies the implicit dependence on the parameter set p and ω^{Th} and ω^{Ref} are the values of the particular property computed using the transfer Hamiltonian and contained in the reference data set respectively. The most fit (those with the smallest error) parameter sets are allowed to produce new parameters in a way which models evolutionary biology, via the exchange of genetic information between two parent individuals through sexual reproduction. Computationally, sexual reproduction is modeled by treating the digits which represent each parameter as genes. A point on each gene is randomly selected, and all the digits to the right of the randomly selected point are interchanged, producing a new parameter. This procedure of fitness assessment and parameter reproduction is repeated until convergence is achieved.

Newton-Raphson Algorithms

These well known methods of optimization [55-56] are gradient following schemes where the function to be minimized is expanded to second order as:

$$f(p) \approx f(p_o) + g^T(p - p_o) + \frac{1}{2}(p - p_o)^T H(p - p_o) \qquad (4.2)$$

The derivative of the error function, equation 4.1, with respect to the parameters cannot be done analytically; therefore, numerical differentiation with respect to each parameter is necessary. Requiring the gradient, g of equation 4.2 to be zero yields

$$(p - p_o) = H^{-1} g \qquad (4.3)$$

which is a prescription for the generation of the new parameter set p from the old set p_o, provided the gradient and Hessian are available. Algorithms which avoid the direct determination of the Hessian matrix by successive approximations are also available [57]. The optimization proceeds with the introduction of a trial parameter set p_o. A new set, p, is generated via equation 4.3 and the procedure continues until the error function is below an acceptable tolerance.

Performance Of Algorithms

GAs and Newton based methods, though they share the same purpose, are computationally very different. Each method has its advantages and disadvantages and as a general recommendation for the success of the optimization, it is recommended to use a combination of the two algorithms.

Perhaps the most marked advantage of the GA over the Newton schemes is the global minimum convergence of the GA versus the Newton algorithms. Since GAs are stochastic optimizations, there is a random "hopping" around the surface which allows the GA to converge to lower minima than Newton schemes which, given an initial point, will proceed downhill and converge locally. Often, Newton schemes get trapped in local minima and have no provision to escape these areas of the surface. Although GAs may sample these local minima which are problematic for Newton schemes, due to the

random nature of the GA search, they can easily escape these areas of the surface and find better solutions.

Although the random search is advantageous as demonstrated in the previous discussion, it has the major drawback that the GA requires lengthy amounts of computer time to converge. A successful GA run requires a large number of trial parameter sets from which to select fit individuals. Further, the GA must be allowed to evolve over many generations so that a suitable set of parameters can be found. In other words, in the spirit of Darwin's theory of natural selection, evolution must be allowed to proceed over many generations in order to find the most fit individual. If the error function which is being minimized can be rapidly evaluated, the requirement of large population size and multiple generation sampling is not detrimental. However, in the parameterization of the transfer Hamiltonian, the error functions are computationally costly, relatively speaking, requiring the evaluation of Hartree-Fock energies and gradients for each parameter set which results in a long run time for the GA.

One final deleterious feature of GAs is that after many generations, if the global minimum has not been located, the search will begin to stagnate. This is due to the successive removal of comparatively less fit individuals from the population, which, after many generations, results in a population of parameter sets which are all more or less equally fit and the evolution of the parameters stalls. This, in a sense, is similar to Newton algorithms getting trapped in a local minimum. When this situation occurs, it is advantageous to switch algorithms and use the Newton optimization algorithm to further reduce the value of the error function. This combination of techniques has been successfully applied in the parameterizations of the transfer Hamiltonian.

Procedure

It is difficult to give a general description of the parameterization procedure for the transfer Hamiltonian since each problem behaves differently and requires problem specific analysis. In general, it has been found that the GA should be initialized with about 100 trial parameter sets and allowed to evolve for 150 to 200 generations. This gives a balance between computational time and sufficient population size for an effective GA run. Using the resulting converged set, the parameters should be refined using the Newton type algorithm to further reduce the value of the error function. For convergence of the optimization, it is always best to focus on a smaller set of reference data. The more types of properties targeted in the parameterization, the worse the transfer Hamiltonian will perform for the target set as a whole. A similar conclusion was reached by Bernstein and Kaxiras in their attempt to parameterize a tight binding Hamiltonian [31].

Transfer Hamiltonian Examples

Since the goal of this work is predictive molecular dynamics simulation which requires accurate interatomic forces, the parameters of the Hartree-Fock variant of the transfer Hamiltonian operator were determined such that the interatomic forces at the transfer Hamiltonian level match those of *ab initio* theory. Specifically, coupled cluster (CCSD/DZP) forces were determined for the dissociation reactions of several small molecules and the parameters determined such that the reference coupled cluster data is reproduced by the transfer Hamiltonian.

Ethane

Coupled cluster forces were determined for the dissociation reaction of ethane,

$$C_2H_6 \leftrightarrow 2CH_3$$

where the carbon-carbon bond is the distinguished coordinate [58]. At each geometry, from the repulsive region out to dissociation, the C-C bond is held fixed and the remaining 3N-7 coordinates allowed to relax. The resulting force curve was then used as reference data for the transfer Hamiltonian.

For this problem, a minimal basis set of valence (s,p) orbitals was assigned to each carbon atom and a single s orbital was used as a basis for each hydrogen. In this particular optimization, only the (a,b,c) parameters of the core repulsion function (see chapter 3, equation 3-21) were determined in the parameterization and the other parameters were held fixed at their given MNDO/AM1 values [59]. The resulting parameters for the core repulsion function are contained in the appendix.

Figure 4-1 is a comparison of the CCSD force curve, versus those obtained with the transfer Hamiltonian and standard semi-empirical theory. In the figure, it is seen that the transfer Hamiltonian parameterization provides an accurate representation of the *ab initio* force curve.

Disilane

A similar parameterization was performed for the dissociation of disilane

$$Si_2H_6 \leftrightarrow 2SiH_3$$

where the Si-Si bond is the distinguished coordinate. Similar to the ethane molecule, forces were generated at the CCSD/DZP level of theory at points in the repulsive and dissociation regions of the potential energy surface, and the core repulsion parameters (AM1 Hamiltonian) determined such that the transfer Hamiltonian forces reproduce those given by coupled cluster theory. The converged parameters are contained in the appendix and the resulting force curves are shown in Figure 4-2.

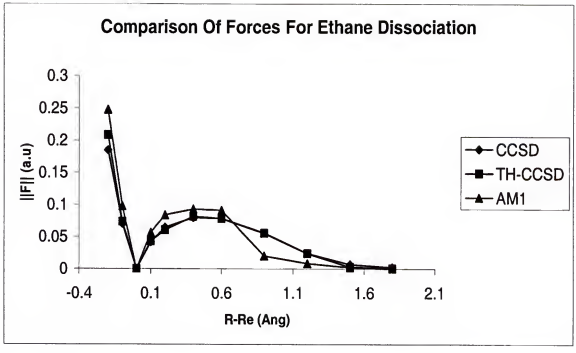

Figure 4-1. Comparison of forces for ethane dissociation using coupled cluster, transfer Hamiltonian, and standard semi-empirical theory.

As figures 4-1 and 4-2 demonstrate, the parameterized forces for the transfer Hamiltonian reproduce those given by the *ab initio* CCSD calculations. It should also be emphasized that the forces are accurate over the whole extent of the potential energy surface, and not just near equilibrium as most of the existing potentials in the literature are. A comparison of the CPU time required for one energy+gradient calculation for the two representative systems is given in Table 4-1. The transfer Hamiltonian performs three to four orders of magnitude more quickly than the *ab initio* model, yet the resulting forces are well reproduced as seen in the figures. This demonstrates that the transfer Hamiltonian provides a convenient route for the inclusion of *ab initio* forces in molecular dynamics simulations.

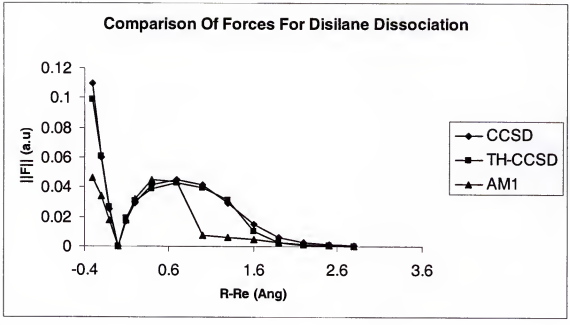

Figure 4-2. Comparison of forces for disilane dissociation using coupled cluster, transfer Hamiltonian, and standard semi-empirical theory.

Conclusion

This chapter discussed the parameterization strategy of the transfer Hamiltonian and presented two test systems which demonstrated the ability of the model to reproduce *ab initio* forces, over a range of geometries, at a much cheaper computational cost than *ab initio* theory. With this as a framework, the remainder of the dissertation will focus on the creation of transfer Hamiltonians for silicon oxide systems and their application to the fracture of a silica model.

Table 4-1. Computer time (CPU seconds) necessary to perform one energy+gradient calculation for the representative systems.

Molecule	CCSD	TH-CCSD
C_2H_6	45.1	0.02
Si_2H_6	104.8	0.02

CHAPTER 5
FRACTURE SIMULATIONS

Introduction

This chapter will discuss the parameterization and validation of a transfer Hamiltonian applicable to the polymorphs of silica. It will be seen that the resulting transfer Hamiltonian performs well for the parameterization cluster, and for clusters outside the realm of the parameterization. This parameterization of the transfer Hamilitonian will then be used in a molecular dynamics simulation of fracture in a silica model containing 108 quantum mechanical atoms.

Fracture

Fracture begins when stress is applied to a material. When the stress exceeds a critical value, atomic bonds begin to break and the crack propagates in the system. The failure of materials due to fracture is a costly and undesirable event which plagues many industries[60]. Therefore, an understanding of the underlying physics and chemistry which determine the macroscopic failure mechanisms in real materials is essential so that premature component failure can be predicted and alleviated.

Fracture may be classified as either brittle or ductile. In general, the primary difference between the two fracture modes is the amount of plastic deformation (degree of atomic disorder) that the material undergoes before fracture occurs. Ductile materials undergo a large degree of plasticity whereas brittle materials show little or no tendency to do so. In ductile materials, once the crack is initiated, it moves slowly and will usually

not extend unless an increased stress is applied. On the contrary, in brittle fracture, cracks spread very rapidly and are accompanied by a low energy release [61].

Typically, it is regarded that ductile fracture is more desirable than brittle fracture in terms of structural or component failure [62]. Since ductile fracture occurs over a period of time and is generally a slower process than brittle fracture, possible sites of material fatigue can be identified and repaired before catastrophic failure.

Transfer Hamiltonian – Silica

Silica is a prototypical brittle material. Given the importance of silica from a geological and technical standpoint, the identification of the mechanical properties of this material has resulted in a significant number of molecular dynamics studies [63-66]. In many of these studies, the BKS or TTAM potentials discussed in the second chapter of this thesis were used to describe the interatomic forces which are the determining factor for a predictive simulation. However, as demonstated previously, these potentials fail to reproduce the forces obtained from high level *ab initio* calculations, therefore results based on these models are questionable. On the contrary, as demonstrated in Chapter 4 for ethane and disilane, the transfer Hamiltonian reproduces coupled cluster theory forces at a fraction of the computational cost of the *ab initio* methods which makes it a useful tool for molecular dynamics and enables a predictive simulation of silica to be performed, given a suitable parameterization. What remains then is a generation of *ab initio* reference data for some small model of silica, the parameterization of the transfer Hamiltonian based on the reference data, and finally, the actual simulation of a much larger sized system using the transfer Hamiltonian as a potential for the dynamics.

Reference Cluster

In the parameterization of any potential, a suitable set of reference data has to be generated and the potential parameters fit such that the reference data is reproduced by the potential. In practice, for molecular dynamics simulations of systems which contain a large number of atoms, a small model of the target simulation system is selected and the relevant properties of the smaller molecule used as a reference data set. After the parameterization, the resulting potential is then assumed to be valid for systems outside the reference data set, such as the target simulation system. Given that assumption, simulations of very large systems can performed using that potential to compute interatomic forces.

In this procedure, it is clear that the choice of parameterization cluster is extremely important. In general, the cluster should provide a good representation of the local geometry of the target simulation system. Silica is known to assume a wide variety of crystal structures such as quartz, cristobalite, coesite, and stishovite. Although the density of each polymorph varies, they all have a region of stability, given the proper ambient conditions. A common feature of all the stable structures is the tetrahedral SiO_4 building unit where a central silicon is surrounded by four oxygen atoms. The tetrahedra share one or more oxygens with neighboring tetrahedra and their relative orientation defines the type of structure. This tetrahedral type of bonding is also present in amorphous silica. Given the importance of the tetrahedral building block in the polymorphs of silica, pyrosilicic acid, $Si_2O_7H_6$ (see Figure 5-1), has been chosen as a small molecular model of bulk silica. This molecule has been used in cluster studies of silica by other researchers as well [67-68].

Figure 5-1. Structure of pyrosilicic acid.

Reference Data For Pyrosilicic Acid

Given the pyrosilicic acid molecule, *ab initio* coupled cluster (CCSD/DZP) calculations were performed to generate the reference data to which the transfer Hamiltonian parameters were fit. For the coupled cluster computations, the p orbital polarization functions of the DZP basis were removed from the hydrogens and the Si-O-Si bond angle was fixed at 180°. The latter restriction was enforced to maintain symmetry and reduce computational effort for the coupled cluster calculations. Initially, the entire system was allowed to relax under the imposed symmetry constraints until an equilibrium configuration was found. Starting from the relaxed geometry, one of the equivalent bridged Si-O bonds was chosen as the distinguished coordinate and the forces, both on the compressive and dissociative sides of the equilibrium bond length, were determined. For the determination of the forces along the distinguished coordinate path, the chosen Si-O bond is held fixed at varying lengths and the other internal degrees of freedom, except those of the hydrogen atoms, allowed to relax. The constraint on the hydrogens was enforced to prevent any spurious hydrogen bonding interactions which would not be present in real silica. The resulting forces from these constrained optimizations are used as reference data for the transfer Hamiltonian. Given an accurate

fit for the *ab initio* forces, the transfer Hamiltonian can then be applied to large molecular dynamics simulations of silica.

Parameterization

For this study, the Hartree-Fock variant of the transfer Hamiltonian was used. A minimal valence basis set (s,p) was assigned to silicon and oxygen in pyrosilicic acid and no polarization functions were assigned to the hydrogen atoms. The one and two electron integrals were computed using the formulas presented in Chapter 3 with the parameters held fixed at their existing values (AM1 parameters) [59,69]. Only the (a,b,c) parameters of the core repulsion function (see equation 3-21) were varied in the optimization. The optimized parameters of the silicon and oxygen atoms in pyrosilicic acid were determined using the genetic and Newton based algorithms such that the coupled cluster forces along the same distinguished coordinate path used in the *ab initio* work was accurately reproduced by the transfer Hamiltonian. The resulting parameter set is contained in the appendix.

Validation Of Potential

Given the converged parameter set, the fidelity of the potential must be examined to ensure that it is indeed reliable. The potential must be able to properly reproduce the given reference data and should also be able to describe systems which were not explicitly considered in the parameterization. Several tests of the current parameterization of the transfer Hamiltonian for silica were conducted and are presented in the following.

Figure 5-2 is a plot of the forces obtained for pyrosilicic acid dissociating into neutral fragments via

$$Si_2O_7H_6 \leftrightarrow {}^{\cdot}OSi(OH)_3 + {}^{\cdot}Si(OH)_3 \qquad (5.1)$$

using coupled cluster, transfer Hamiltonian and BKS potentials. In the figure it is seen that the transfer Hamiltonian reproduces the coupled cluster forces in the repulsive and dissociative regions of the potential energy surface, unlike the classical potential. This is an important feature since these potentials are used to study fracture where interatomic bonds are stretched from their equilibrium values and need proper description over the entire range of bond lengths.

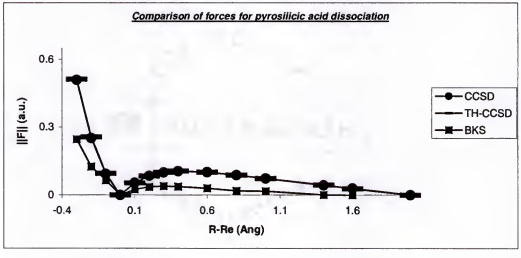

Figure 5-2. Comparison of forces for dissociation of pyrosilicic acid into neutral fragments using *ab initio* and parameterized potentials.

The forces plotted in figure 5-2 pertain to the lower energy dissociation pathway of pyrosilicic acid into neutral fragments and the reference data to which the transfer Hamiltonian parameters were fit was determined for this particular dissociation path. However, the system may also separate into charged fragments via

$$Si_2O_7H_6 \leftrightarrow {}^{-}OSi(OH)_3 + {}^{+}Si(OH)_3 \qquad (5.2)$$

where the different pathways can be studied computationally by using a restricted (charged) or unrestricted (neutral) Hartree-Fock computation to generate the ground state reference determinant. Dissociation into charged species lies ≈30 kcal/mol higher in energy than the neutral dissociation and as a test on the veracity of the parameter set

obtained for this model cluster, the transfer Hamiltonian forces for the charged dissociation were compared to those computed with coupled cluster theory. A plot of the forces for the dissociation into charged fragments is shown in Figure 5-3. There it is seen that the coupled cluster forces for dissociation into charged fragments are recovered by the transfer Hamiltonian, although the parameterization only included data from the lower energy pathway. This type of flexibility is not possible with a classical potential such as BKS or TTAM which does not recognize the difference between ions and neutral species.

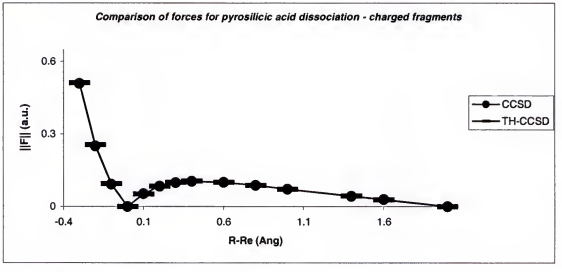

Figure 5-3. Comparison of forces for pyrosilicic acid dissociation into charged fragments.

The potential energy surface of the two dissociation pathways is shown in Figure 5-4. The energy differences for the transfer Hamiltonian were obtained by integration of the forces computed with the converged parameter set. As the figure demonstrates, the potential energy surface along each pathway is reproduced by the transfer Hamiltonian although no explicit consideration of energies was included in the parameterization.

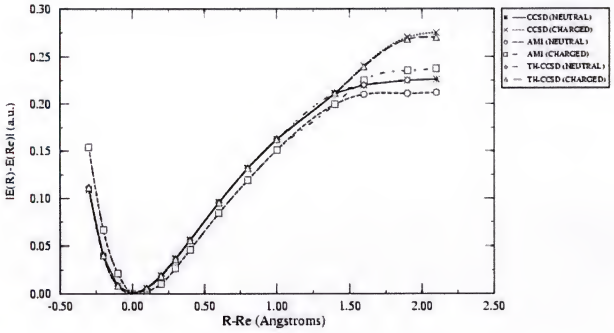

Figure 5-4. Comparison of potential energy surfaces for pyrosilicic acid dissociation into neutral and charged fragments using coupled cluster, transfer Hamiltonian and standard semi-empirical theory.

In order for the transfer Hamiltonian to be applicable to large polymorphs of silica, it is necessary that the parameters be convergent with respect to cluster choice. In other words, the parameters which were determined for pyrosilicic acid must not change (significantly) if the next larger sized Si-O cluster, trisilicic acid, is used for the parameterization. If the parameters are indeed convergent, then it can be argued that the potential is applicable to larger Si-O systems of all sizes. This is achievable in the context of the transfer Hamiltonian because the operator is very short ranged (limited to two center interactions at most) and the interatomic interactions fall off very rapidly with distance. Therefore, the inclusion of additional Si-O units which are long distances from the site of interest have a nominal effect on the local forces. To exemplify this, consider Figure 5-5 which is a comparison of the forces for trisilicic acid, which contains one more SiO_4 unit than does the pyrosilicic acid parameterization cluster. Due to the larger cluster size, this system was treated with DFT, however, the resulting potential energy surface and forces should closely follow those that would be obtained with coupled cluster theory. As shown, the transfer Hamiltonian force curve generated with parameters determined for a smaller cluster, is a good representation of the larger cluster forces. This would also apply for even larger clusters of SiO_4 units due to the local nature of the transfer Hamiltonian and is evidence that this potential is applicable to bulk silica samples.

The CPU time required for each energy+gradient evaluation using pyrosilicic acid is shown in Table 5-1. The computational time for the *ab initio* coupled cluster calculation is 4 orders of magnitude more costly than the transfer Hamiltonian computation although the forces and energy differences are equivalent in both models.

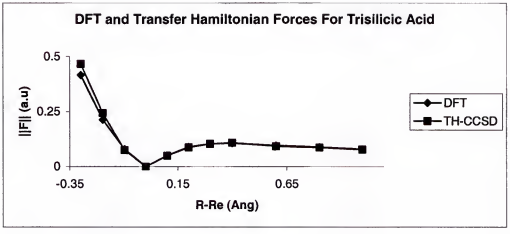

Figure 5-5. Comparison of forces for trisilicic acid.

Although the transfer Hamiltonian performs quickly enough for use in simulations, as shown in the table, the classical BKS potential is still much faster than the transfer Hamiltonian. The simplicity of the classical potential form renders it extremely fast and the transfer Hamiltonian, although a step in the right direction, will never be able to compete with the must simpler classical potential forms in regard to computational speed.

Table 5-1. Computer time (CPU seconds) necessary to perform one energy+gradient calculation for the pyrosilicic acid system.

Method	CPU Time (s)
CCSD	8656
DFT	375
Transfer Hamiltonian	0.17
BKS	0.001

As stated previously, for potentials of both quantum and classical forms, it is ***assumed*** that the converged parameter set is valid for systems outside the realm of the reference data set. This assumption has to be made because it is obviously impossible to include every possible situation in one parameterization. Although this "leap of faith" is

unavoidable, it is still important to assess the applicability of the potentials to systems which differ from that to which they were parameterized. A faithful potential should be able to handle a variety of bonding situations, especially potentials which are used to study silica. The surface of amorphous silica is known to contain many defect sites which includes under coordinated silicon atoms and small, highly strained rings. A predictive simulation of silica must use a potential which is capable of properly characterizing all these bonding patterns.

Figure 5-6 contains histograms detailing the error between bond lengths and angles in several small silicon oxide systems different from pyrosilicic acid. In comparison to CCSD(T) geometries, the transfer Hamiltonian performs very well for these systems, although none, some of which contain double bonds, were included in the parameterization set. Also shown in the figure is the geometric error obtained with the TTAM and LSU 3-body potential. The error in these internal coordinates using these potentials is greater than that with the transfer Hamiltonian, and the LSU potential fails to produce the linear bond arrangement in the triatomic molecule SiO_2. This is due to the preferential treatment of tetrahedral bond angles built into the LSU potential (see Chapter 2).

As a final test on the robustness of the parameterization, the transfer Hamiltonian was applied to a class of systems known as polyhedral oligomeric silsesquioxanes POSS). These cage-like silicon-oxide molecules are closely related to silica and silicones and have shown great promise as additives which greatly improve the thermal and physical properties of many plastics [70]. Xiang *et al.* [71] performed a DFT study (of several of these systems, and presented the structure and energy ordering for POSS

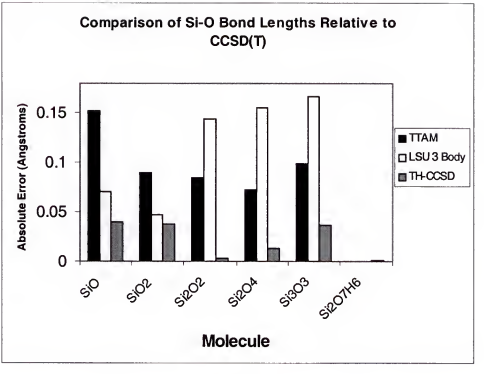

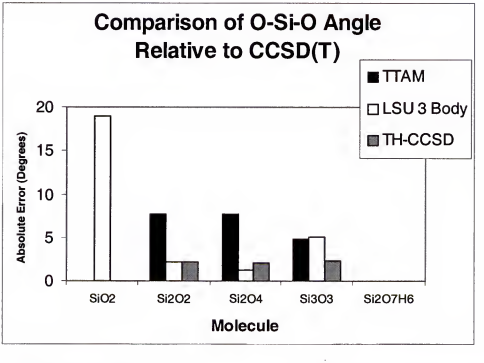

Figure 5-6. Comparison of bond lengths and angles for several small silicon oxide systems using various potentials.

isomers with equivalent stoichiometries. The eight and twelve silicon atom cages shown in Figure 5-7 were treated with the transfer Hamiltonian to determine if the energy ordering among the isomers given by DFT was reproduced by the transfer Hamiltonian.

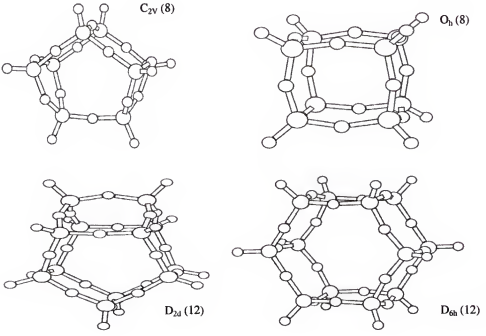

Figure 5-7. Structure of the eight and twelve member POSS cages. The isomers are labeled by their point group symmetries and number of silicon atoms in each cage.

Xiang *et al.* report that among the two eight member isomers, the conformer of O_h symmetry is the most stable. For the twelve member cage, the D_{2d} isomer is the most favorable geometry. The transfer Hamiltonian reproduces these structures and energetic orderings.

Given the performance of the transfer Hamiltonian in the tests given above, it can be concluded that the transfer Hamiltonian is a useful tool for the study of silica. The forces for pyrosilicic acid match those of coupled cluster theory in the repulsive and bond

break regions which is necessary for fracture simulations. Further, the description of other silicon oxide systems of different coordinations is well described which is necessary to properly model defect sites in silica.

Application

The transfer Hamiltonian was used to study the failure response to uniaxial tension of a 108 atom silicon-oxide nanorod (Figure 5-8) via molecular dynamics simulation. The nanorod is a model system of silica which is large enough to yield genuine materials properties such as stress-strain curves yet can be treated fully quantum mechanically at the transfer Hamiltonian level.

The nanorod, as shown in the figure, consists of planar six membered rings, Si_6O_6. Each planar ring shares, both above and below, a ring of oxygen atoms with adjacent six member rings. To alleviate any dangling bonds, the nanorod is terminated with capped rings where each silicon atom of the terminating ring is connected by a bridging oxygen or two interstitial oxygens as shown. The nanorod has the proper stoichiometric ratio of silicon to oxygen observed in real silica (1:2) and is considered to be a viable model for the study of silica. In this particular work, the nanorod was used to elucidate the differences, if any, of the fracture mode of the nanorod using classical versus quantum potentials.

Fracture Of Nanorod

Before presentation of the simulations and as an additional demonstration of the faithful applicability of the transfer Hamiltonian to large systems, the energy of the nanorod was computed at equilbrium and strained geometries using the transfer Hamiltonian and density functional theory. The nanorod was equilibrated with each potential and successively expanded by a few percent to generate the energy profiles

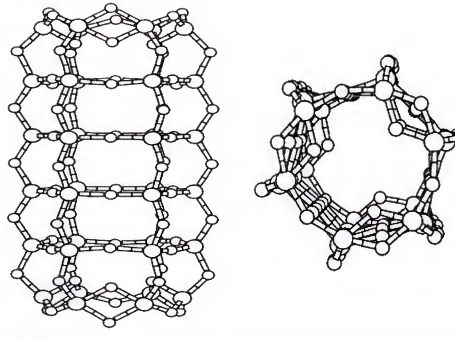

Figure 5-8. 108 atom silica nanorod viewed from side and top. The larger circles are silicon atoms and the others are oxygen.

shown in Figure 5-9. The potential curves show fairly good agreement considering the initial parameterization focused on accurate forces for a much smaller cluster. Although the agreement with DFT is good, the transfer Hamiltonian operates much more quickly. Each single point computation required 43 CPU seconds for the transfer Hamiltonian, while the DFT computations used 85,000 seconds of CPU time.

To study fracture, the nanorod was subjected to uniaxial tension using molecular dynamics simulation where the stress was applied by fixing the longitudinal movement of the fifteen atoms contained in the caps on both ends of the nanorod. With the long axis of the nanorod considered to be the z axis, each end cap atom was given a fixed velocity in the loading direction (along z axis) and the remaining atoms allowed to relax, with their positions computed by the deterministic molecular dynamics algorithms. The simulations were conducted at a constant temperature of 1K using the predictor-corrector algorithm, where the temperature was maintained by velocity rescaling [3,4].

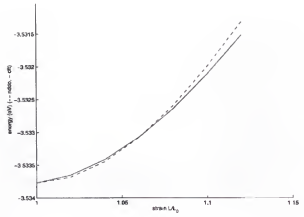

Figure 5-9. Plot of potential energy curves for the nanorod using transfer Hamiltonian and density functional potentials.

The stress-strain curve obtained for fracture of the nanorod using the transfer Hamiltonian is shown in Figure 5-10. Curves obtained using BKS and TTAM classical potentials are included for comparison. The stresses plotted in the figure correspond to the sum of all forces parallel to the loading direction in the constrained atoms of the end caps divided by the projected cross sectional area of the end caps. The cross sectional area is updated at each time step and accounts for any effects due the xy motion of the atoms in the longitudinally constrained end caps. This differs from the usual engineering stress-strain curve where the initial cross sectional area is used at each time step. The strain is computed as $(L-L_o)/L_o$, where L and L_o are the current and initial lengths of the nanorod respectively.

Examination of the stress-strain curves indicates that the transfer Hamiltonian and classical potentials predict approximately equivalent values for the critical strain, however the tensile strengths for the transfer Hamiltonian and BKS potentials are higher

than those predicted with the TTAM potential. The curvature of the classical potential curves indicates that the nanorod undergoes a more plastic deformation, characteristic of ductile fracture, than that of the transfer Hamiltonian which maintains an essentially linear stress-strain relationship (brittle fracture) up to failure.

The qualitatively distinct fracture modes indicated by the classical (ductile) and quantum potential (brittle) exemplifies the importance of having accurate forces in the dynamics simulation. It cannot be concluded which failure mode is actually correct, but given the performance of the transfer Hamiltonian for the tests discussed previously, the results it yields for the nanorod should be considered the most reliable. The failure of the classical potentials to properly characterize the mechanical behavior of the nanorod could, were the nanorod of technological importance, result in wasted time and effort for experimentalists due to misleading recommendations by simulators. Of course this is a hypothetical situation at present, however, the implications are clear.

Hybrid Dynamics Of Nanorod

The CPU time required for the nanorod simulations is presented in Table 5-2. The quantum simulations require much more time to reach completion than do the classical potentials. This difference will become even more pronounced as the size of the simulation system increases and the quantum calculation becomes swamped by the huge dimension of the matrices involved in the calculation. This situation can be rectified by the use of a hybrid molecular dynamics scheme whereby the forces of interaction are computed using the much more rapid classical potential and the slower transfer Hamiltonian in the same simulation.

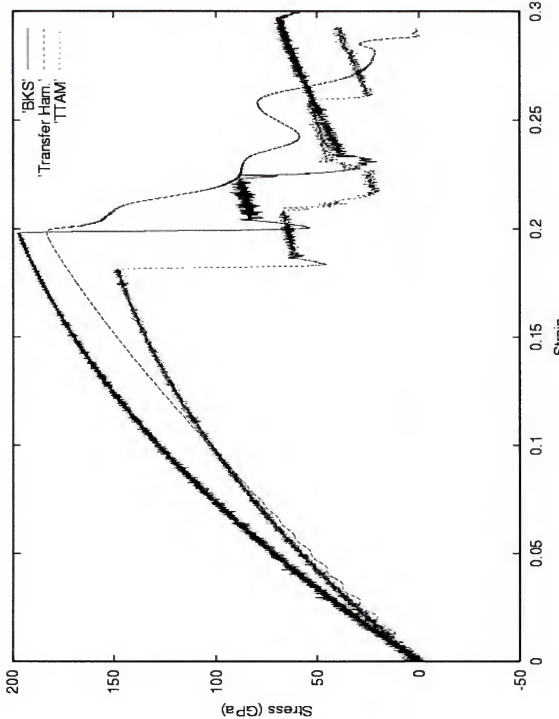

Figure 5-10. Stress-Strain curves for uniaxial tension of 108 atom nanorod.

Table 5-2. Computer time (CPU seconds) necessary to perform 5000 timestep MD simulation.

Potential	CPU Time
Transfer Hamiltonian	2.5 Days
TTAM/BKS	1.5 Minutes

In the hybrid simulation scheme, the transfer Hamiltonian is used to compute the force vector, F_{TH}, at the current configuration. Those forces are stored and the classical potential force vector, F_{CL}, at the same configuration is determined. The difference between the two, $F_{ERR}=F_{TH}-F_{CL}$, is a vector of errors between the quantum forces and the classical forces. Given these errors, the classical potential is used to generate forces for the next few configurations and the previously determined quantum corrections are added to each component of the classical force vector at each time step. This scheme has the advantage that fewer of the more costly transfer Hamiltonian calculations need to be performed since the majority of the time steps are evaluated with the much faster classical potential.

The accuracy of this force correction scheme was assessed by simulating the fracture of the nanorod, as before, but using the classical TTAM potential with periodic force corrections from the transfer Hamiltonian. Three simulations were performed where the transfer Hamiltonian force corrections were evaluated at intervals of 10, 25, and 50 time steps. The resulting stress-strain curves are shown in Figures 5-11 through 5-13, as a function of the frequency of quantum corrections performed in the simulation. As the figures show, the force-corrected TTAM results are closer to the pure transfer Hamiltonian curve, although the scheme does introduce a large amount of numerical

"noise." As the frequency of quantum corrections increases, the force-corrected TTAM simulation approaches that of the transfer Hamiltonian more closely, the limit being a quantum correction at each timestep, i.e. a fully quantum simulation.

Given the decreased number of time steps for which the transfer Hamiltonian potential must be evaluated, the hybrid simulation gives a dramatic speedup in computational time, as shown in Table 5-3 which lists the CPU time required for each simulation.

Conclusion

This chapter discussed the parameterization and validation of a transfer Hamiltonian applicable to silica. It was shown that the potential is accurate for the parameterization cluster and other silicon-oxide systems outside the parameterization set, including POSS systems. The fracture mode of a 108 atom silicon oxide nanorod was simulated and the transfer Hamiltonian yielded a qualitatively different material behavior than did the classical BKS and TTAM potentials. Finally, a computationally efficient hybrid simulation scheme was presented wherein the classical force fields are updated with quantum information which yields a decreased simulation time and congruent stress-strain curves.

Table 5-3. CPU time for hybrid simulations.

Force Correction Interval (Timesteps)	**CPU Time**
0 (Fully Quantum)	2.5 Days
10	1.6 Hours
25	1 Hour
50	1/2 Hour

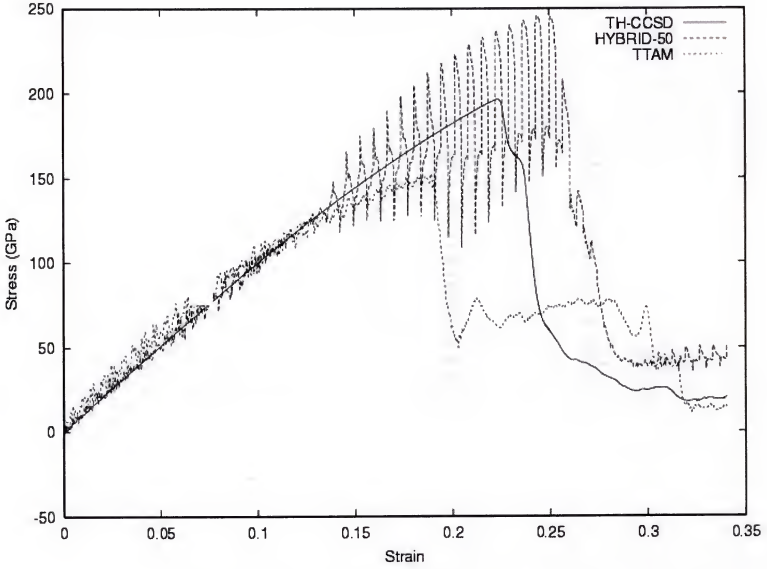

Figure 5-11. Stress strain curves using a quantum force correction every 50 timesteps.

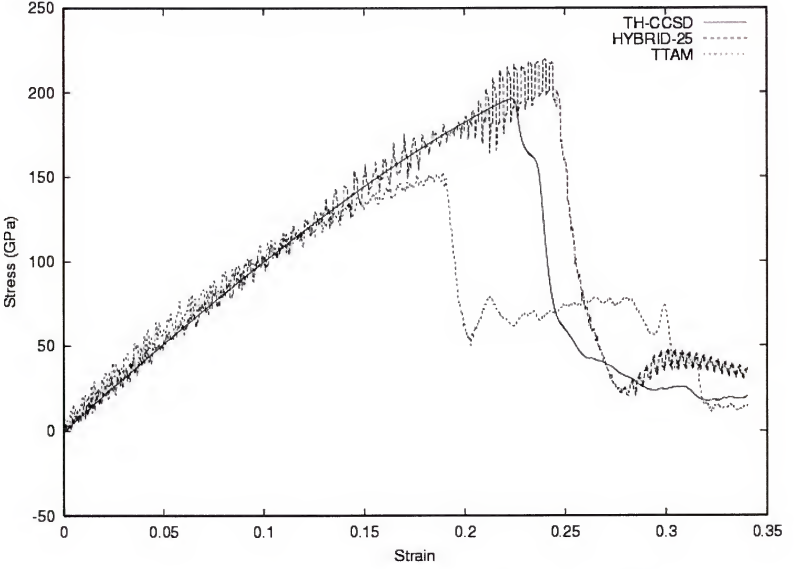

Figure 5-12. Stress strain curves using a quantum force correction every 25 timesteps.

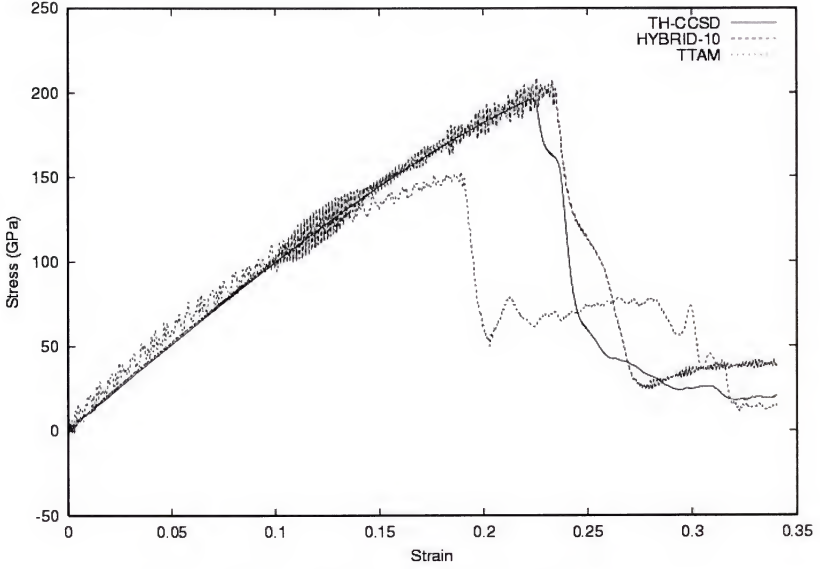

Figure 5-13. Stress strain curve using quantum correction every 10 timesteps.

CHAPTER 6
HYDROLYTIC WEAKENING

Introduction

This chapter will discuss the changes in the mechanical properties of silica in the presence of water by a phenomena known as hydrolytic weakening. A recently presented mechanism for this process is outlined and encoded into the parameters of a transfer Hamiltonian. The transfer Hamiltonian will then be used in molecular dynamics simulations of water assisted fracture of the nanorod and silicon-oxide rings.

Hydrolytic Weakening

It is well known that water greatly enhances the rate of crack growth in silica in a process known as hydrolytic weakening [72]. Although the mechanism of this process is still under debate, it is generally accepted that this is a stress induced phenomenon whereby water assists the rupture of Si-O bonds in the silica structure and enhances the fracture process. One model of this process, due to Michalske and Freiman [73], identifies the water monomer as the primary mediator of water assisted rupture of silicon-oxygen bonds in silica. In this mechanism, it is suggested that a single water molecule orients a lone pair of electrons on its oxygen towards a silicon atom of the surface. A subsequent proton transfer from water to an oxygen of the silica surface results in rupture of the surface Si-O bond and enhanced crack tip propagation.

The Michalske-Freiman model has been examined by Lindsay et al. [68] who applied Hartree-Fock level calculations to pyrosilicic acid in the presence of several molecules, including water and ammonia. Their work indicates that the approach of the

monomer, in the manner described by Michalske and Freiman, is favorable, however the conclusions given in the paper are limited by the computational methodology applied to the test system.

To further elucidate the water assisted bond rupture process, Del Bene *et al.* [74] applied large basis set, correlated methods to $H_3SiOSiH_3$ in the presence of the water monomer, dimer, and trimer. In this work, it was found that the binding energies of the water clusters with the $H_3SiOSiH_3$ increased in the order monomer<trimer<dimer which indicates that the water dimer interacts more favorably with the Si-O bond than does the monomer used in the Michalske-Freiman model. Del Bene *et al.* also identified a mechanism of Si-O bond rupture using the water dimer. In this scheme, two of the protons in $H_3SiOSiH_3$ were replaced by fluorine atoms (see Figure 6-1) to model the effect of the bulk in large silica samples. As the Si-O bond was stretched, a dual proton transfer occurred which mediated the rupture of the bond as outlined in the figure. Given this mechanism for water assisted bond cleavage in silica, what remains is the encoding of this information into a transfer Hamiltonian parameter set and the demonstration of the process by molecular dynamics simulation.

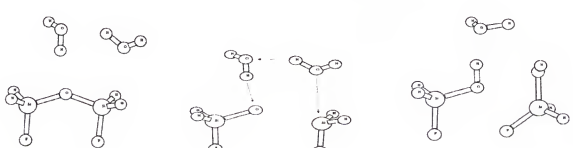

Figure 6-1. Schematic representation of dual proton transfer mechanism.

Transfer Hamiltonian

Parameterization

To successfully simulate the interaction of water with silica given the mechanism described above, the forces which describe water-water, water-silica, and silica-silica interactions have to be described quantitatively. The transfer Hamiltonian described in Chapter 5 only characterizes the silica-silica interactions and does not accurately reproduce the interactions of silica with water, therefore a reparameterization is necessary.

The parameterization of this mechanism is very difficult given the requirements imposed upon the transfer Hamiltonian parameter set. In this case, as for the previous systems, accurate molecular dynamics is the goal therefore the parameterization will focus on accurate reproduction of *ab initio* forces for dissociation of water, and silica in the presence of water. The water molecules are composed of oxygen/hydrogen atoms and silica contains silicon/oxygen. Therefore, there are three atomic species which are available for parameterization. This parameterization can proceed in two ways. First, the entire reference data set (forces) for the water-water and water-silica interactions can be targeted in one huge parameterization run which includes water and the water-silica cluster forces at several geometries. An alternative is to parameterize the water cluster interaction separately, and then, with the fixed oxygen/hydrogen parameters, determine the silicon parameters for the silica model cluster. The latter option is favorable because although two successive optimizations must be performed, the target data set is smaller for each run and yields improved convergence.

Proceeding in this manner, converged oxygen/hydrogen parameters were determined which reproduce coupled cluster (CCSD) geometries, dipole moments, and

forces for the water monomer and dimer using the Hartree-Fock variant of the transfer Hamiltonian. The MBPT(2) forces for the silica model (Figure 6-1) were then fit by variation of the silicon parameters using fixed values for the oxygen/hydrogen parameters. The transfer Hamiltonian description of oxygen and silicon includes addition of spherical harmonic d functions and a set of p functions for each hydrogen in addition to the usual minimal basis, valence set of basis functions. The AM1 core repulsion function was also included to increase the flexibility of the fit in the core terms. The converged parameter set is contained in the appendix.

Validation

Selected internal coordinates and the dipole moments for the water monomer/dimer are contained in Table 6-1 where it is seen that the CCSD geometry of the monomer and dimer is well reproduced by the transfer Hamiltonian. The computed dipole moment for the monomer is accurate but that for the dimer is in error by 0.2D.

Table 6-1. Selected internal coordinates for the water monomer and dimer. The CCSD values are given in parenthesis. All values in Angstroms, degrees, and Debye.

Coordinate	Monomer	Dimer
R(OH)	0.96(0.95)	0.96(0.95)
θ(HOH)	105(104)	105(102)
$\theta(HOH)_B$		100(101)
R(OO)		2.90(2.90)
Dipole	1.85(1.86)	2.45(2.68)

Figure 6-2 is a plot of the forces for dissociation of the water monomer using the transfer Hamiltonian and coupled cluster theory for the reaction

$$H_2O \leftrightarrow OH+H \qquad (6.1)$$

The transfer Hamiltonian accurately reproduces the coupled cluster forces in both the repulsive and dissociative regions of the potential energy surface which is required for the proton transfer to be modeled accurately.

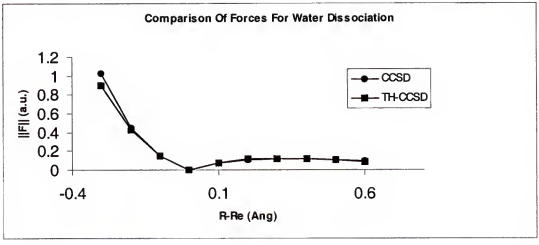

Figure 6-2. Comparison of forces for dissociation of water monomer.

Figure 6-3 is a plot of the forces for dissociation of the silica model used by Del Bene *et al.* as shown in Figure 6-1, where the broken Si-O bond is treated as the distinguished coordinate. The force curve resulting from the transfer Hamiltonian is a fairly good representation of the second order curve. However, the fit is not as good as seen for the other systems. This is due to the reduced number of parameters available for this parameterization. Recall that only the silicon parameters are variable for the fit because those of the oxygen/hydrogen are fixed by the water parameterization.

Simulations Of Hydrolytic Weakening

Given the transfer Hamiltonian parameterization for water+silica, two molecular dynamics simulations were performed which demonstrate the process of hydrolytic

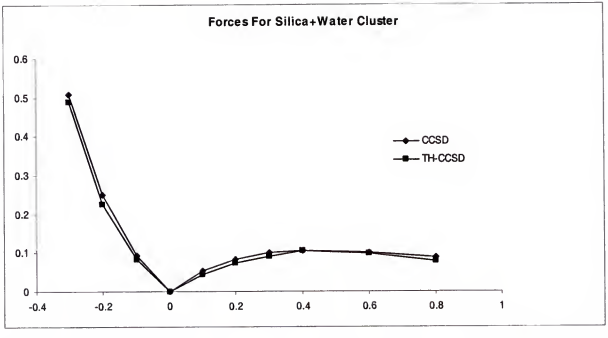

Figure 6-3. Comparison of forces for dissociation of fluorinated silica model using CCSD and TH-CCSD potentials.

weakening. In the first, a small SiO_2 ring was subjected to radial strain in the presence of the water dimer. The second simulation involved the nanorod which was strained uniaxially as before, but with water included. The stress-strain curves resulting from both simulations show a marked decrease in tensile strength in the presence of water which is an example of hydrolytic weakening.

Hydrolytic Weakening In Silica Ring

Recent investigations indicate that small, highly strained two-rings exist at the surface of amorphous and crystalline silica [75]. Due to high strain energy in these rings, they readily hydrolyze in the presence of water and are the sites at which water will preferentially attack the silica surface. Bromley *et al.* [76] suggested a hierarchy of silica rings and chains as models of extended silica surfaces due to the agreement between the computed molecular ring vibrational frequencies and IR bands measured on silica

surfaces. As an initial test for the transfer Hamiltonian, a fracture simulation of the ten member $(SiO_2)_{10}$ ring from Bromley *et al.* (Figure 6-4) in the presenece of the water dimer was performed using the transfer Hamiltonian. In this simulation, strain was imposed by prescribing a fixed radial velocity to each silicon atom and allowing the remaining atoms to relax at each time step.

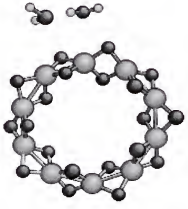

Figure 6-4. Ten member silica ring with water dimer. The large circles are silicon and the smaller are oxygen and hydrogen atoms.

Snapshots of the initial, intermediate, and final configurations of the simulation are shown in Figure 6-5 where it is seen that the dual proton transfer mechanism of Del Bene *et al.* does indeed occur in the simulation. The effect of the water dimer on the strength of the ring can be observed in Figure 6-6 which is a plot of the radial component of the force summed over the ten silicon atoms. This type of plot is analogous to a stress-strain curve which would require division by a cross sectional area normal to the loading direction which does not exist for the radially stressed silica ring. The strength of the molecular ring is smaller in the presence of water due to the water assisted rupture of the Si-O bond of the ring which exemplifies hydrolytic weakening.

Figure 6-5. Initial, intermediate, and final stages of the simulation.

Hydrolytic Weakening in Nanorod

The nanorod introduced in Chapter five was also used to demonstrate hydrolytic weakening. In this simulation, a defect notch was placed in the nanorod by removal of an oxygen atom as shown in Figure 6-7. This was done so that the water dimer would have a preferential site of attack when in the vicinity of the defect and, as before, uniaxial strain was applied to the 15 atoms in the end caps at the top and bottom of the nanorod. This simulation contained 113 quantum mechanical atoms with 997 basis functions in total and required approximately 6 days of computer time to complete.

Snapshots of the initial, intermediate, and final stages of the simulation are shown in Figure 6-8 and, as for the molecular ring, the dual proton transfer mechanism is seen to occur. A plot of the stress-strain curves for the full, notched, and notched+water nanorods is shown in Figure 6-9. There, it is seen that the full rod is weakened by the introduction of the defect and even moreso in presence of water.

Conclusion

This chapter discussed the phenomenon known as hydrolytic weakening where the strength of silica is reduced in the presence of water. A proposed mechanism for the process was outlined and a transfer Hamiltonian parameterized which modeled the *ab*

initio forces for the water monomer/dimer, and silica in the presence of water. Two exemplary simulations were presented which demonstrate the proton transfer mechanism and show that the strength of the silica models used is diminished when water is present.

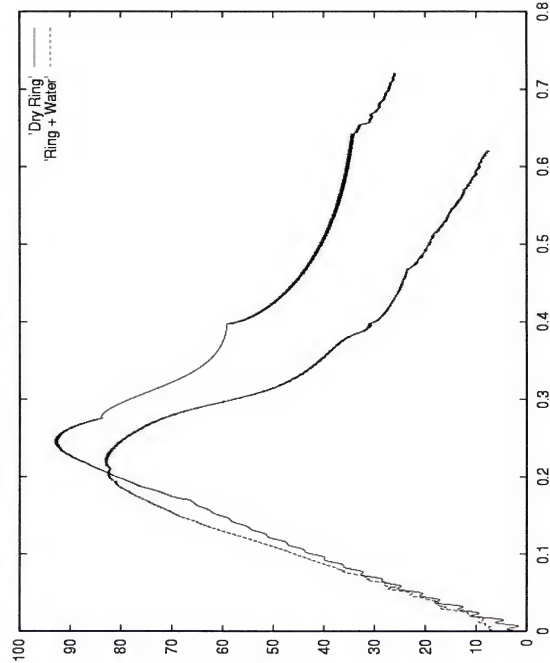

Figure 6-6. Plot of radial stress for ring and ring+water.

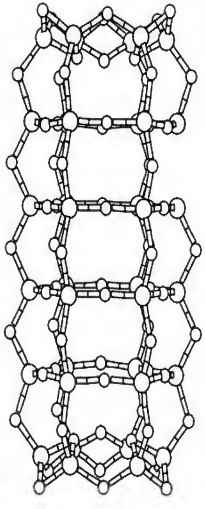

Figure 6-7. Nothced nanorod.

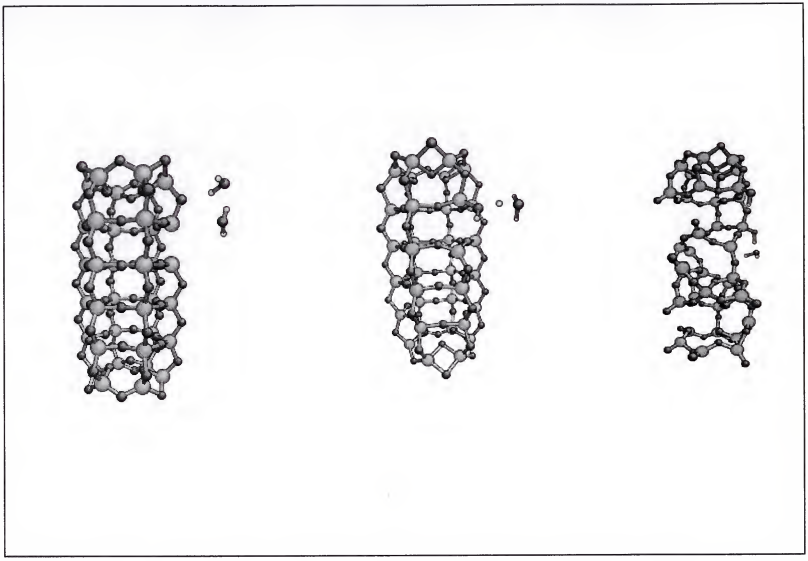

Figure 6-8. Initial, intermediate, and final stages of nanorod+water simulation.

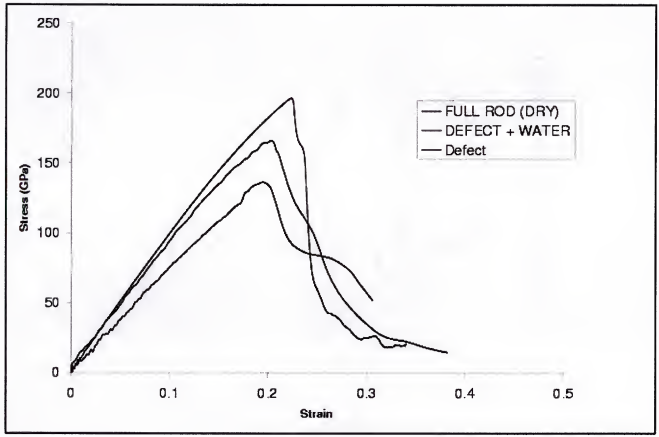

Figure 6-9. Stress strain curves for nanorod and nanorod+water dimer.

APPENDIX
CONVERGED PARAMETER VALUES

Table A-1. AM1 core repulsion parameters for ethane transfer Hamiltonian.

FN11	H	0.119189531
FN21	H	5.000296781
FN31	H	1.187005328
FN12	H	-5.3083007877155D-02
FN22	H	5.000124589
FN32	H	1.804518427
FN13	H	-9.0847048920079D-02
FN23	H	2.000275061
FN33	H	2.099731286
FN11	C	7.3065280087242D-02
FN21	C	4.997496108
FN31	C	1.54935964
FN12	C	3.4458410577681D-02
FN22	C	4.999451186
FN32	C	1.881061799
FN13	C	-3.7607845486172D-02
FN23	C	4.994770304
FN33	C	2.088195795
FN14	C	1.1448481218013D-02
FN24	C	5.001200215
FN34	C	2.682312427

Table A-2. AM1 core repulsion parameters for silane transfer Hamiltonian.

FN11	H	0.137564937
FN21	H	5.000159773
FN31	H	1.196210001
FN12	H	-9.4826688340866D-04
FN22	H	5.000003974
FN32	H	1.798502571
FN13	H	-3.3202209151372D-02
FN23	H	2.000166665
FN33	H	2.097608564
FN11	SI	0.2578874
FN21	SI	8.99972034
FN31	SI	0.925522328
FN12	SI	6.1808735024902D-02
FN22	SI	5.009880484
FN32	SI	1.675096047
FN13	SI	-7.2005255197313D-02
FN23	SI	5.000113621
FN33	SI	3.194398939

Table A-3. AM1 core repulsion parameters for pyrosilicic acid/silica transfer Hamiltonian.

FN11	Si	0.244008364
FN21	Si	9.001939022
FN31	Si	0.864725617
FN12	Si	4.1292711037864D-02
FN22	Si	5.000018741
FN32	Si	1.949114673
FN13	Si	-4.8092512969194D-04
FN23	Si	4.999732104
FN33	Si	2.972359776
FN11	O	0.217315862
FN21	O	4.978545859
FN31	O	0.818795183
FN12	O	4.2716100192577D-02
FN22	O	6.999606981
FN32	O	1.526792547

Table A-4. MNDO/d + AM1 core repulsion parameters for water monomer/dimer transfer Hamiltonian.

UDD	8	-15.67446636
BETAD	8	-10.49396769
ZD	8	0.932435114
ZSN	8	1.25677511
ZPN	8	1.244652126
ZDN	8	1.934697891
UPP	1	-1.567965104
BETAP	1	-0.270500345
ZP	1	7.88E-02
GSP	1	7.327374489
GPP	1	3.626974692
GP2	1	2.820302283
HSP	1	1.186342464
ALPHA	8	3.278924663
ALPHA	1	2.867667176
A1	8	-0.786143499
B1	8	6.182851647
C1	8	0.951527347
A2	8	1.255861236
B2	8	8.633959981
C2	8	2.244723778
A1	1	1.032905318
B1	1	4.805637752
C1	1	1.960955941
A2	1	-0.947660325
B2	1	4.419691962
C2	1	2.03102124

LIST OF REFERENCES

1. M. Karplus and J. A. McCammon, Nature Structural Biology **9,** 646 (2002).

2. B.J. Alder and T.W. Wainwright, J. Chem. Phys. **27**, 1208 (1957).

3. J. M. Haile, *Molecular Dynamics Simulation,* John Wiley and Sons, New York, 1992.

4. M.P Allen and D.J. Tildesley, *Computer Simulation Of Liquids*, Clarendon Press, Oxford,1987.

5. V. E. Lamberti, L. D. Fosdick, E.R. Jessup, and C. Schauble, J. Chem. Ed. **79**, 601 (2002).

6. L. Verlet, Phys. Rev. **159**, 98 (1967).

7. C.W. Gear, *Numerical Initial Value Problems In Ordinary Differential Equations,* Prentice Hall, Englewood Cliffs, 1971.

8. J. Tersoff, Phys. Rev. B **37**, 6991 (1988).

9. B.W.H. van Beest, G.J. Kramer, and R.A. van Santen, Phys. Rev. Lett. **64**, 1955 (1990).

10. S. Tsuneyuki, M. Tsukada, H. Aoki, and Y. Matsui, Phys. Rev. Lett. **61**, 869 (1988).

11. A.J. Stone, *The Theory Of Intermolecular Forces*, Clarendon Press, Oxford, 1996.

12. A. Szabo and N.S. Ostlund, *Modern Quantum Chemistry,* McGraw-Hill, New York, 1989.

13. A.E. Reed and F. Weinhold, J. Chem. Phys. **83**, 735 (1985).

14. A.E. Reed and F. Weinhold, J. Chem. Phys. **78**, 4066 (1983).

15. S. Subramanian and S. Yip, Comp. Mat. Sci. **23**, 116 (2002).

16. T. Zhu, J. Li, S. Yip, R.J. Bartlett, S.B. Trickey, and N.H. Leeuw, Mol. Sim. **29**, 671 (2003).

17. R.J. Bartlett and J.F. Stanton (1993). Applications Of Post-Hartree-Fock Methods: A Tutorial. In K.B. Lipkowitz and D.B. Boyd (eds.) *Reviews In Computational Chemistry – Volume 5* (1-119). New York: VCH Publishers.

18. A. E. Carlsson, Solid State Phys. **43**, 1 (1990).

19. D. Holland and M. Marder, Adv. Mat. **11**, 793 (1999).

20. F. H. Stillinger and T. A. Weber, Phys. Rev. B **31**, 5262 (1985).

21. F.A. Cotton, G. Wilkinson, and P.L. Gaus, *Basic Inorganic Chemistry*, John Wiley and Sons, New York,1995.

22. B. W. Dodson, Phys. Rev. B **33**, 7361 (1986).

23. R. Biswas and D.R. Hamann, Phys. Rev. B **36**, 6434 (1987).

24. J. Tersoff, Phys. Rev. B **37**, 6991 (1988).

25. W. Andreoni and G. Pastore, Phys. Rev. B **41**, 10243 (1990).

26. P. Vashishta, R.K. Kalia, J.P. Rino, and I. Ebbsjo, Phys. Rev. B **41**, 12197 (1990).

27. R. Car and M. Parrinello, Phys. Rev. Lett. **55**, 2471 (1985).

28. J. Simons, *An Introduction To Theoretical Chemistry*, Cambridge University Press, Cambridge, 2003.

29. C. M. Goringe, D. R. Bowler, and E. Hernandez, Rep. Prog. Phys. **60**, 1447 (1997).

30. B. K. Panda, S. Mukherjee, and S. N. Behera, Phys. Rev. B **63**, 045404 (2001).

31. N. Bernstein and E. Kaxiras, Phys. Rev. B **56**, 10488 (1997).

32. I. Kwon, R. Biswas, C.Z. Wang, K.M. Ho, and C.M. Soukoulis, Phys. Rev. B **49**, 7242 (1994).

33. T.J. Lenosky, J.D. Kress, I. Kwon, A.F Voter, B. Edwards, D.F. Richards, S. Yang, and J.B. Adams, Phys. Rev. B **55**, 1528 (1997).

34. Y. Hsiao, K. Runge, M.G. Cory, and R.J. Bartlett, J. Phys. Chem. A **105**, 7004 (2001).

35. J. Stewart (1990). Semiempirical Molecular Orbital Methods. In K.B. Lipkowitz and D.B. Boyd (eds.) *Reviews In Computational Chemistry – Volume 1* (45-81). New York: VCH Publishers.

36. G. Klopman and R.C. Evans (1977). The Neglect Of Differential Overlap Methods Of Molecular Orbital Theory. In G. Segal (ed) *Modern Theoretical Chemistry* (29-67). New York: Plenum Press.

37. W. Thiel, Theo.- J. Mol. Str. **398**, 1 (1997).

38. R.G. Parr and W. Yang, *Density Functional Theory Of Atoms And Molecules*, Oxford University Press, Oxford, 1989.

39. T.D. Crawford and H.F. Schaefer III (2000). An Introduction To Coupled Cluster Theory For Computational Chemists. In K.B. Lipkowitz and D.B. Boyd (eds.) *Reviews In Computational Chemistry – Volume 14* (33-136). New York: VCH Publishers.

40. G.E. Scuseria, Chem. Phys. Lett. **226**, 251 (1994).

41. C.H. Martin and K.F. Freed, J. Chem. Phys. **100**, 7454 (1994).

42. P.O. Lowdin, J. Math. Phys. **3**, 969 (1962).

43. P.O. Lowdin, J. Math. Phys. **6**, 1341 (1965).

44. P. Gill, B.G. Johnson, J.A. Pople, and M.J. Frisch, Chem. Phys. Lett. **197**, 499 (1992).

45. T. Helgaker, J. Olsen, P. Jorgensen, *Molecular Electronic Structure Theory,* John-Wiley and Sons, New York, 1995.

46. F. Jensen, *Introduction To Computational Chemistry,* John Wiley and Sons, New York, 1999.

47. I. N. Levine, *Quantum Chemistry*, Prentice-Hall, New Jersey, 1991.

48. See www.cachesoftware.com/mopac/Mopac2002manual/node441.html. Site accessed March 12, 2003.

49. J.C. Slater, *Quantum Theory Of Atomic Structure*, Mc-Graw-Hill, New York, 1960.

50. M.J.S. Dewar and W. Thiel, Theo. Chim. Acta. **46**, 89 (1977).

51. G. Klopman, J. Am. Chem. Soc. **86**, 4550 (1964).

52. D. Feller and E. R. Davidson (1990). Basis Sets For Ab Initio Molecular Orbital Calculations And Intermolecular Interactions. In K.B. Lipkowitz and D.B. Boyd (eds.) *Reviews In Computational Chemistry – Volume 1* (1-44). New York: VCH Publishers.

53. R. P. Sherman and R. Grinter, J. Mol. Str. – Theo. **135**, 127 (1986).

54. D. E. Goldberg, *Genetic Algorithms In Search, Optimization, And Machine Learning,* Addison-Wesley, New Jersey,1989.

55. J. Stoer and R. Bulirsch, *Introduction To Numerical Analysis,* Springer-Verlag, New York, (1980).

56. J. D. Head and M.C. Zerner, Int. J. Quan. Chem. **33**, 177 (1988).

57. W.H Press, B.P. Flannery, S. A. Teukolsky, and W. T. Vetterling, *Numerical Recipes*, Cambridge University Press, Cambridge, 1986.

58. I. Rossi and D. G. Truhlar, Chem. Phys. Lett. **233**, 231 (1995).

59. M.J.S Dewar, E.G. Zoebisch, E.F. Healy, and J.J.P Stewart, J. Am. Chem. Soc. **107**, 3902 (1985).

60. See www.mech.gla.ac.uk/Research/Fracture. Site accessed March 9, 2003.

61. See www.sv.vt.edu/classes/MSE2094_NoteBook/97ClassProj/exper/bailey/www/bailey.html. Site accessed March 9, 2003.

62. See www.tpub.com/content/doe/h1017v2/css/h1017v2_35.htm. Site accessed March 9, 2003.

63. K. Trachenko and M.T. Dove, J. Phys. – Cond. Matt. **14**, 7449 (2002).

64. S. Subramanian and S. Yip, Comp. Mat. Sci. **23**, 116 (2002).

65. M..S. Somayazulu, S.M. Sharma, and S.K. Sikka, Phys. Rev. Lett. **73**, 98 (1994).

66. R.G. Dellavalle and E. Venuti, Chem. Phys. **179**, 411 (1994).

67. M.D. Newton, M. O'Keefe, and G.V. Gibbs, Phys. Chem. Minerals **6**, 305 (1980).

68. C. G. Lindsay, G. S. White, S.W. Freiman, and W. Wong-Ng, J. Am. Ceram. Soc. **77**, 2179 (1994).

69. M.J.S. Dewar and C. Jie, Organomet. **1**, 1486 (1987).

70. See www.reade.com/Products/Polymeric/poss.html. Accessed March 9, 2003.

71. K.H. Xiang, R. Pandey, U.C. Pernisz, and C. Freeman, J. Phys. Chem. B **102**, 8704 (1998).

72. S.M. Wiederhorn, J. Am. Ceram. Soc. **50**, 407 (1967).

73. T.A. Michalske and S.W. Freiman, J. Am. Ceram. Soc. **66**, 284 (1983).

74. J.E. Del Bene, K. Runge, and R.J. Bartlett, Comp. Mat. Sci. **27**, 102 (2003).

75. D. Ceresoli, M. Bernasconi, S. Iarlori, M. Parrinello, and E. Tosatti, Phys. Rev. Lett. **84**, 3887 (2000).

76. S.T. Bromley, M.A. Zwijnenburg, and Th. Maschmeyer, Phys. Rev. Lett. **90**, 035502 (2003).

BIOGRAPHICAL SKETCH

The author was born in Columbus, Ohio in 1974. At the age of 10, he moved with his family to Chesterfield, Virginia, just 5 miles south of the state capital, Richmond. During his sophomore year at Thomas Dale High School, the author joined the cross-country team which resulted in his receiving a full athletic scholarship to the University of Virginia which he attended from 1993-1997.

While at the University of Virginia he was introduced to quantum chemistry by his undergraduate research advisor, Dr. Michal Sabat. With the encouragement of Dr. Sabat, he decided to pursue a graduate degree in the field which brought him to the University of Florida and the Quantum Theory Project in the summer of 1998.

I certify that I have read this study and that in my opinion it conforms to acceptable standards of scholarly presentation and is fully adequate, in scope and quality, as a dissertation for the degree of Doctor of Philosophy.

Rodney J. Bartlett, Chairman
Graduate Research Professor of Chemistry

I certify that I have read this study and that in my opinion it conforms to acceptable standards of scholarly presentation and is fully adequate, in scope and quality, as a dissertation for the degree of Doctor of Philosophy.

Nils Yngve Ohrn
Professor of Chemistry

I certify that I have read this study and that in my opinion it conforms to acceptable standards of scholarly presentation and is fully adequate, in scope and quality, as a dissertation for the degree of Doctor of Philosophy.

Jeffrey Krause
Associate Professor of Chemistry

I certify that I have read this study and that in my opinion it conforms to acceptable standards of scholarly presentation and is fully adequate, in scope and quality, as a dissertation for the degree of Doctor of Philosophy.

David E. Richardson
Professor of Chemistry

I certify that I have read this study and that in my opinion it conforms to acceptable standards of scholarly presentation and is fully adequate, in scope and quality, as a dissertation for the degree of Doctor of Philosophy.

James Wellons Dufty
Professor of Physics

This dissertation was submitted to the Graduate Faculty of the Department of Chemistry in the College of Liberal Arts and Sciences and to the Graduate School and was accepted as partial fulfillment of the requirements for the degree of Doctor of Philosophy.

May 2004

_____

Dean, Graduate School